

Improved gravitational waveforms from spinning black hole binaries

Edward K. Porter^{1,2} and B. S. Sathyaprakash¹

¹*School of Physics and Astronomy, Cardiff University,
5, The Parade, Cardiff, Wales, UK, CF24 3YB and*

²*Laboratoire de l'Accélérateur Linéaire, B.P. 34,
Bâtiment 208, Campus d'Orsay, 91898 Orsay Cedex, France*

The standard post-Newtonian approximation to gravitational waveforms, called T-approximants, from non-spinning black hole binaries are known not to be sufficiently accurate close to the last stable orbit of the system. A new approximation, called P-approximants, is believed to improve the accuracy of the waveforms rendering them applicable up to the last stable orbit. In this study we apply P-approximants to the case of a test-particle in equatorial orbit around a Kerr black hole parameterized by a spin parameter q that takes values between -1 and 1 . In order to assess the performance of the two approximants we measure their *effectualness* (i.e. larger overlaps with the exact signal), and *faithfulness* (i.e. smaller biases while measuring the parameters of the signal) with the exact (numerical) waveforms. We find that in the case of prograde orbits, that is orbits whose angular momentum is in the same sense as the spin angular momentum of the black hole, T-approximant templates obtain an effectualness of ~ 0.99 for spins $q \lesssim 0.75$. For $0.75 < q < 0.95$, the effectualness drops to about 0.82 . The P-approximants achieve effectualness of > 0.99 for all spins up to $q = 0.95$. The bias in the estimation of parameters is much lower in the case of P-approximants than T-approximants. We find that P-approximants are both effectual and faithful and should be more effective than T-approximants as a detection template family when $q > 0$. For $q < 0$ both T- and P-approximants perform equally well so that either of them could be used as a detection template family.

I. INTRODUCTION

Stellar mass compact binaries consisting of double neutron stars (NS), double black holes (BH) or a mixed binary consisting of a neutron star and a black hole, are the primary targets for a direct first detection of gravitational waves (GW) by interferometric detectors, LIGO [1], VIRGO [2], GEO600 [3], and TAMA [4]. Under radiation reaction the orbit of a binary slowly decays, emitting a signal whose amplitude and frequency increases with time and is termed a “chirp” signal. While it is believed that there is a greater population of NS-NS binaries [5, 6, 7, 8, 9], it is the BH-BH binaries that are the strongest candidates for detection since they can be seen from a greater volume, about two orders-of-magnitude greater than NS-NS binaries [5, 10].

A. Matched filtering

In order to detect such sources one employs the method of matched filtering [11]. Briefly, the method works as follows: Firstly, one creates a set of waveforms, or templates as they are called, that depend on a number of parameters of the source and its location and orientation relative to the detector. These templates are then cross-correlated with the detector output weighted by the inverse of the noise spectral density. If a signal, whose parameters are close to one of the template waveforms, is actually present in the detector output then the cross-correlation builds up, with the dominant contribution coming from frequencies where the noise spectral density is low. Thus, in the presence of a sufficiently strong signal the correlation will be much larger than the RMS correlation in the absence of any signal. How large should it be before we can be confident about the presence of a signal depends on the combination of the rate of inspiral events and the false alarm probability (see e.g. Ref. [12] for a simple estimation).

The effectiveness of matched filtering depends on how well the phase evolution of the waveform is known. Even tiny instantaneous differences, as low as one part in 10^3 in the phase of the true signal that might be present in the detector output and the template that is used to dig it out could lead to a cumulative difference of several radians since one integrates over several hundreds to several thousands of cycles. In view of improving the signal-to-noise ratio for inspiral events there has been a world-wide effort in accurately computing the dynamics of a compact binary and the waveform it emits or to use phenomenologically defined detection template families [13, 14, 15].

B. Phasing of the coalescing binary signal

There have been parallel efforts on using two different approximation schemes: On the one hand the post-Newtonian (PN) expansion of Einstein's equations has been used to treat the dynamics of two bodies of comparable masses with and without spin, in orbit around each other. This approximation is applicable when the velocities involved in the system are small but there is no restriction on the ratio of the masses [16, 17, 18, 19, 20, 21, 22].

On the other hand, black hole perturbation theory has been used to compute the dynamics of a test particle in orbit around a spin-less or spinning black hole. Black hole perturbation theory does not make any assumptions on the velocity of the components, but is valid only in the limit when the mass of one of the bodies is much less than the other [23, 24, 25, 26, 27, 28].

The post-Newtonian approximation is a perturbative method which expands the equations of motion, binding energy and GW flux as a power series in v/c , where v is a typical velocity in the system and c is the speed of light. In the early stages of an inspiral, the radiation reaction time-scale $\tau_{\text{RR}} \sim \omega/\dot{\omega}$, where ω is the angular velocity and $\dot{\omega}$ its time-derivative, is much greater than the orbital time-scale $\tau_{\text{orb}} \sim 1/\omega$. It is during this adiabatic regime that the post-Newtonian approximation works best. At present, the PN expansion for the case of comparable-masses is known to order $\mathcal{O}(v^6)$ [21] and $\mathcal{O}(v^7)$ [22], for the energy and flux functions, respectively. However, at this order an arbitrary parameter exists in the expression for the flux. In order to see how well PN theory performs, we can compare two different systems. If we assume a NS-NS binary of masses $(1.4, 1.4) M_{\odot}$ and a lower frequency cutoff of the detector at 40 Hz, then the ‘‘orbital velocity’’ of the binary is small, $v \sim 0.12$, [59] when it enters the detector bandwidth and the two stars are still largely separated, $r \sim 70 M$. The ratio of time-scales in the most sensitive regime of the detector is in the range $4.5 \times 10^3 \leq \tau_{\text{RR}}/\tau_{\text{orb}} \leq 680$. If on the other hand we take a BH-BH binary of masses $(10, 10) M_{\odot}$, the orbital velocity is quite large, $v \sim 0.23$, and the separation is quite small, $r \sim 19 M$, upon entering the detector bandwidth. This is very close to the regime, $v \sim 0.3$, $r \sim 11 M$, where the background curvature becomes strong and the motion relativistic. Once again, comparing time-scales, we obtain $140 \leq \tau_{\text{RR}}/\tau_{\text{orb}} \leq 40$, where the final value is taken at the last stable orbit at $f_{\text{LSO}} \sim 210$ Hz. It is known that PN theory becomes inaccurate at an orbital separation of $r \leq 10 M$ [29]. Therefore, post-Newtonian approximation becomes less valid for higher mass systems in the LIGO band but well describes the early stages of the inspiral of a NS-NS system visible in LIGO.

As previously stated, black hole perturbation theory makes no assumptions about the orbital velocity of the components, but does restrict their masses. One assumes that a test particle of mass μ is in orbit about a central BH of mass M such that $\mu \ll M$. Assuming this restriction is satisfied we have an analytical expression for the energy. However, no analytical expression has been worked out for the gravitational wave flux emitted by such a system. Using black hole perturbation theory, a series approximation was initially calculated to $\mathcal{O}(v^3)$ by Poisson for a test particle in circular orbit around a Schwarzschild black hole [23]. The series was extended numerically to $\mathcal{O}(v^5)$ by Cutler et al. [24], and then to $\mathcal{O}(v^8)$ by Tagoshi and Nakamura [25] and confirmed analytically by Tagoshi and Sasaki [27]. The most recent progress is an extension of the series to $\mathcal{O}(v^{11})$ by Tagoshi, Tanaka and Sasaki [28]. For a test particle in circular orbit about a Kerr black hole, the initial progress was again made by Poisson [30]. The series approximation was improved from $\mathcal{O}(v^3)$ to $\mathcal{O}(v^5)$, and subsequently to $\mathcal{O}(v^8)$, by Tagoshi, Tanaka, Shibata and Sasaki [31, 32].

Several authors [28, 33, 34, 35, 36] have shown that the convergence of both post-Newtonian approximation and black hole perturbation theory is too slow to be useful in constructing accurate templates. More recently, Damour, Iyer and Sathyaprakash (hereafter DIS) showed for the case of a test-mass in orbit about a Schwarzschild BH, that by using properly defined energy and flux functions that have better analytical properties, combined with Padé techniques, it was possible to take the existing series expansion and improve its convergence properties [36]. The new approximation in which Padé approximants of new energy and flux functions are used to derive improved templates is called P-approximant. Using a fiducially defined ‘‘exact’’ waveform, it was shown that the P-approximant templates were both more *effective* (i.e. larger overlaps with the exact waveform) and *faithful* (i.e. larger overlaps with the exact waveform and lower biases in the estimation of parameters) than the corresponding post-Newtonian (hereafter T-approximant) templates. While in general, more templates are needed for P-approximant templates to cover the same volume of parameter space [37], the extra computational cost is preferred for the increased performance in P-approximants. The failure of the PN expansion to converge sufficiently quickly in the case of a test particle orbiting a Schwarzschild BH [38] does not bode well for the modelling of even a test particle inspiralling into a Kerr BH. Another motivation for this work is that at present there is effort to use *effective one body* (EOB) waveforms [39, 40] to detect the inspiral and merger signals from two comparable-mass Kerr BHs in GW data. As the EOB waveforms are based partially on P-approximants, any development and concretization of the benefits of P-approximant templates will boost our confidence in using these improved waveforms as detection templates.

C. Organisation of the paper

In this paper we will extend the P-approximant technique to the case of a test particle orbiting a Kerr black hole. The reason for focusing on test-mass systems is that we can use the exact numerical fluxes [52] from black hole perturbation theory with which to compare our results and thereby reliably demonstrate the usefulness of the technique. We begin in Sec. II with a summary of the matched filtering and the signal-to-noise ratio achieved by the first generation of GEO, LIGO and VIRGO interferometers for spinning black hole binaries.

We then go on to discuss in Sec. III the current state-of-the-art in our understanding of the evolution of a test particle in orbit around a Kerr black hole. In particular, we shall discuss the time-evolution of the orbital energy and gravitational wave flux as a function of the spin of the central black hole at various post-Newtonian orders, and the locations of the last stable and unstable circular orbits. We shall see that the post-Newtonian expansion of the flux does not show a regular behaviour as we move from low to high orders in the post-Newtonian expansion, becoming worse for more rapidly spinning black holes. In order to improve the convergence properties of the flux function, in Sec. III E we shall introduce a modified form of the flux function and its Padé approximant. We shall demonstrate in Sec. IV the improved behaviour of the Padé approximant, at first graphically and then by showing that the overlaps, of the inspiral waveform based on it with the exact waveform, are close to unity. We shall use a number of different test systems in our comparison: These will range from systems with dissimilar masses, such as a NS-BH binary, to comparable-mass systems, such as a BH-BH binary. To deal with the comparable mass systems, we shall introduce in the energy and flux functions a term dependent on the symmetric mass ratio $\eta \equiv m_1 m_2 / M^2$. While not being entirely consistent, because of the fact that no finite mass correction terms are included, it allows us to examine the performance of various templates as we move from the test-mass systems to comparable-mass systems.

The emphasis of the current paper is also on the estimation of parameters. We have carried out a detailed study of how good T- and P-approximants are in measuring the parameters of the binary. We shall show in Sec. IV that as a result of not being *effectual* representations of the exact signal, T-approximants also turn out not to be *faithful* representations either. In other words, the systematic error in the estimation of the parameters caused by the wrong phasing of the signal is much larger in the case of T-approximants than in the case of P-approximants. In summary, P-approximants are not only *effectual* but they are *faithful* too as in the case of non-spinning black hole binaries.

II. WAVEFORM AND SIGNAL-TO-NOISE RATIO

In this Section we will discuss the nature of the post-Newtonian waveform from an inspiralling compact binary and the response of an antenna to such a signal. We will then use the Fourier transform of the waveform to compute the signal-to-noise ratio (SNR) that can be achieved for these signals when they are detected using matched filtering.

A. The Waveform

In the transverse-traceless gauge gravitational waves are represented by two polarisation amplitudes h_+ and h_\times . The response $h(t)$ of an antenna to an incoming signal is expressed as a combination of the two polarisation states and the beam pattern functions F_+ and F_\times of the antenna as [43]: $h(t) = h_+ F_+ + F_\times h_\times$. For a wave from a binary of masses m_1 and m_2 (total mass $M = m_1 + m_2$ and mass ratio $\eta = m_1 m_2 / M^2$) that is inclined with respect to the plane of the sky at an angle i , propagating in the direction $(\theta, \bar{\phi})$, (see Ref. [43] for exact definitions), frequency F and polarization angle $\bar{\psi}$ with respect to the antenna, the polarisation amplitudes, in the so-called *restricted* post-Newtonian approximation [33], are

$$h_+(t; M, \eta, i) = \frac{4\eta M}{d} \frac{(1 + \cos^2 i)}{2} v_F^2(t) \cos \phi(t), \quad (1)$$

$$h_\times(t; M, \eta, i) = \frac{4\eta M}{d} \cos i v_F^2(t) \cos \phi(t), \quad (2)$$

with $v_F = (\pi M F)^{1/3}$ a velocity parameter, and the beam-pattern functions are

$$F_+(\theta, \bar{\phi}, \bar{\psi}) = \frac{1}{2} (1 + \cos^2 \theta) \cos 2\bar{\phi} \cos 2\bar{\psi} - \cos \theta \sin 2\bar{\phi} \sin 2\bar{\psi}, \quad (3)$$

$$F_\times(\theta, \bar{\phi}, \bar{\psi}) = \frac{1}{2} (1 + \cos^2 \theta) \cos 2\bar{\phi} \sin 2\bar{\psi} + \cos \theta \sin 2\bar{\phi} \cos 2\bar{\psi}. \quad (4)$$

Using the above expressions for the beam-pattern functions and gravitational wave amplitudes the response takes the form

$$h(t) = \frac{4\eta M}{d} \mathcal{C} v_F^2(t) \cos[\phi(t) + \phi_0], \quad (5)$$

where the amplitude coefficient \mathcal{C} and phase ϕ_0 can be assumed to be constant for signals lasting for a short duration (say, less than about 30 mins):

$$\mathcal{C} = \frac{1}{2} \sqrt{(1 + \cos^2 i)^2 F_+^2 + 4(\cos i)^2 F_\times^2}, \quad (6)$$

$$\phi_0 = \tan^{-1} \left[\frac{2F_\times \cos i}{F_+(1 + \cos^2 i)} \right]. \quad (7)$$

Thus, gravitational wave antennas are not able to extract the two polarisations separately and the data analysis problem boils down to matching the time-varying phase $\phi(t)$, and to a lesser extent the amplitude v_F^2 , of the antenna response function.

Post-Newtonian theory and the quadrupole formula applied to a binary give the relativistic binding energy $E(v_F)$ per unit mass, and the flux of the waves $\mathcal{F}(v_F)$ as series expansions in the parameter v_F . Once we have the binding energy and the flux we can use the energy balance argument, namely that the flux of gravitational waves is completely balanced by the negative rate of change of the binding energy [$M dE(v_F)/dt = -\mathcal{F}(v_F)$], in order to arrive at a parametrized equation for the evolution of the phase $\phi(t)$ of gravitational waves. Integrating the energy balance equation supplemented by $2\pi F = d\phi/dt$, one obtains:

$$t(v_F) = t_{\text{ref}} + M \int_{v_F}^{v_{\text{ref}}} dv \frac{E'(v)}{\mathcal{F}(v)}, \quad (8)$$

$$\phi(v_F) = \phi_{\text{ref}} + 2 \int_{v_F}^{v_{\text{ref}}} dv v^3 \frac{E'(v)}{\mathcal{F}(v)}, \quad (9)$$

where $E'(v_F) = dE(v_F)/dv_F$, t_{ref} is a reference time and ϕ_{ref} is a reference phase of the signal, when the velocity parameter is $v_F = v_{\text{ref}}$. The numerical integration of the above equations is more economical when the following differential equations are solved instead,

$$\frac{dv_F}{dt} = -\frac{\mathcal{F}(v_F)}{ME'(v_F)}, \quad \frac{d\phi}{dt} = \frac{2v_F^3}{M}. \quad (10)$$

The parametric representation, Eqs. (8) and (9), of the phasing formula $\phi = \phi(t)$ holds under the assumption of ‘adiabatic inspiral’, *i.e.*, that gravitational radiation damping can be treated as an adiabatic perturbation of a circular motion. However, the effective one-body approach [39, 40, 41, 42] has allowed a treatment of the radiation damping to proceed beyond the adiabatic approximation. In order to extract an inspiral signal that may be buried in noisy data by the method of matched filtering, we need to employ post-Newtonian accurate representations for the two functions $E'(v_F)$ and $\mathcal{F}(v_F)$ that appear in the above phasing formulas. Given an approximant $E_A(v_F)$, $\mathcal{F}_A(v_F)$, one can define by replacing $E(v_F) \rightarrow E_A(v_F)$, $\mathcal{F}(v_F) \rightarrow \mathcal{F}_A(v_F)$ in Eqs. (8) and (9) some approximate parametric representation, $t = t_A(v_F)$, $\phi = \phi_A(v_F)$, and therefore a corresponding approximate template

$$h^A = h^A(t; \mathcal{C}, t_{\text{ref}}, \phi_{\text{ref}}, M, \eta), \quad (11)$$

obtained by replacing v_F , in the following v_F -parametric representation of the waveform

$$h^A(v_F) = \frac{4\eta M}{d} \mathcal{C} v_F^2 \cos \phi_A(v_F), \quad (12)$$

by the function of time $v_F = v_A(t)$ obtained by inverting $t = t_A(v_F)$.

There are several ways of performing this inversion which leads to the different T-approximants, *TaylorT1* [keep the rational polynomial $E'(v_F)/\mathcal{F}(v_F)$ in Eqs. (8) and (9) as is and solve the integrals numerically], *TaylorT2* [re-expand the rational polynomial as a post-Newtonian series, truncate terms to the appropriate order and solve the integrals analytically to get series expansions, $t = \sum_k t_k v_F^k$ and $\phi = \sum_k \phi_k v_F^k$, but solve numerically for $\phi(t)$ from the parametric equations] and *TaylorT3* [do as in TaylorT2 but also invert the series expansions to obtain the phasing as an explicit function of time: $\phi(t) = \sum_k \phi_k (t_{\text{ref}} - t)^{-k/8}$], as discussed in Ref. [41].

It is often convenient to deal with the Fourier representation of the waveform. In the stationary phase approximation the Fourier transform, defined as $\tilde{h}(f) = \int_{-\infty}^{\infty} h(t) \exp(2\pi i f t) dt$, for positive frequencies reads [43, 44, 45, 46]

$$\tilde{h}(f) \equiv \int_{-\infty}^{\infty} h(t) \exp(2\pi i f t) dt = \frac{2\eta M C}{d} \frac{v_f^2}{\sqrt{\dot{F}}} e^{i[\psi(f) - \frac{\pi}{4}]}, \quad (13)$$

and, since $h(t)$ is real, $\tilde{h}(-f) = \tilde{h}^*(f)$. Here t_f is the stationary point of the phase ψ (i.e., t_f is defined by $d\psi/dt|_{t_f} = 0$), $v_f = (\pi M f)^{1/3}$, \dot{F} is the time-derivative of the instantaneous gravitational wave frequency evaluated at the stationary point given by,

$$\dot{F} = -\frac{3v_f^2}{\pi M^2} \frac{\mathcal{F}(v_f)}{E'(v_f)}, \quad (14)$$

and $\psi(f) = 2\pi f t_f - \phi(t_f)$ is the phase of the Fourier transform in the stationary phase approximation given by

$$\psi(f) = 2\pi i f t_{\text{ref}} - \phi_{\text{ref}} + 2 \int_{v_f}^{v_{\text{ref}}} (v_f^3 - v^3) \frac{E'(v)}{\mathcal{F}(v)} dv. \quad (15)$$

Instead of solving the integrals in the above equation it is numerically efficient to solve the following equivalent differential equations for the phasing formula in the Fourier domain:

$$\frac{d\psi}{df} - 2\pi t = 0, \quad \frac{dt}{df} + \frac{\pi M^2 E'(f)}{3v_f^2 \mathcal{F}(f)} = 0. \quad (16)$$

And in this study we have used the above differential equations in computing the waveforms. For the energy we have used the exact analytical formula (see next Section); for the flux we have used the exact numerical flux to define the exact waveform and the perturbative expansions, or their re-summed improved versions, to define the approximate waveforms.

B. Signal-to-Noise Ratio

In order to estimate the signal-to-noise ratio (SNR) we shall assume that the signal is detected using matched filtering and that the bank of templates used in matched filtering has a waveform that matches the unknown signal very closely. To compute the optimum SNR we need to know the noise spectral density of the detectors. For initial LIGO, the one-sided noise power spectral density (PSD) from the design study [1] is given by [46]

$$S_h(f) = 9 \times 10^{-46} [0.52 + 0.16x^{-4.52} + 0.32x^2] \text{ Hz}^{-1}, \quad (17)$$

where $x \equiv f/f_k$, and $f_k = 150 \text{ Hz}$ is the ‘‘knee-frequency’’ of the detector. We take the PSD to be infinite below the lower frequency cutoff of $f_{\text{low}} = 40 \text{ Hz}$. For the VIRGO detector the PSD is given by

$$S_h(f) = 3.24 \times 10^{-46} [10^3(25x)^{-5} + 2/x + 1 + x^2] \text{ Hz}^{-1}, \quad (18)$$

where $f_k = 500 \text{ Hz}$ and $f_{\text{low}} = 20 \text{ Hz}$. Finally, for the GEO detector the expected noise PSD is [60]

$$S_h(f) = 10^{-46} \times [(3.4x)^{-30} + 34/x + 20(1 - x^2 + x^4/2)/(1 + x^2/2)] \text{ Hz}^{-1} \quad (19)$$

where $f_k = 150 \text{ Hz}$ and the noise is assumed to be infinite below a lower frequency cutoff of $f_{\text{low}} = 40 \text{ Hz}$.

Next, let us define the scalar product of two waveforms h and g by

$$\langle a | b \rangle = 2 \int_0^{\infty} \frac{df}{S_h(f)} \left[\tilde{h}(f) \tilde{g}^*(f) + \tilde{h}^*(f) \tilde{g}(f) \right], \quad (20)$$

where the $*$ denotes complex conjugate and $\tilde{h}(f)$, $\tilde{g}(f)$ are the Fourier transforms of $h(t)$, $g(t)$. The (square) of the signal-to-noise ratio obtained by matched filtering a signal h with a template g is given by

$$\rho^2 \equiv \left(\frac{S}{N} \right)^2 = \frac{\langle h | g \rangle^2}{\langle g | g \rangle}. \quad (21)$$

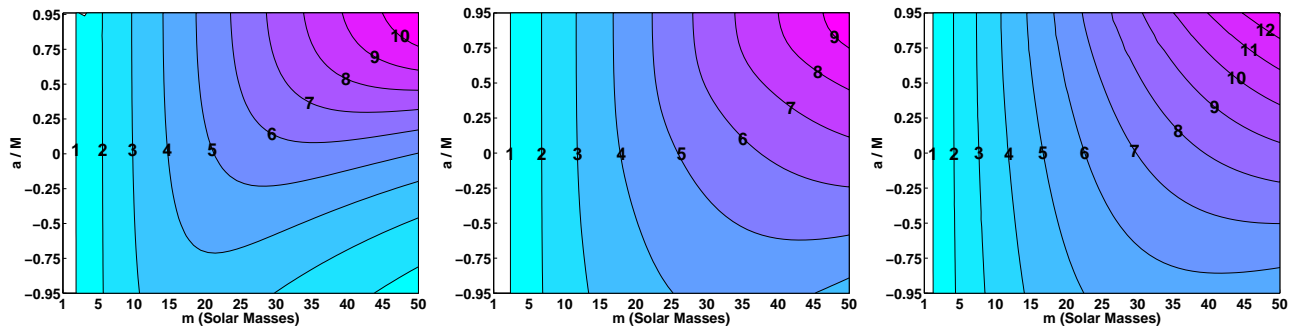


FIG. 1: The RMS SNR for equal mass binaries at 100 Mpc for the LIGO (left), GEO (center) and VIRGO (right) antennas.

If the template perfectly matches the signal then the SNR is simply $\rho^2 = \langle h, h \rangle$. For the inspiral signal given in Eq. (13), and using the *Newtonian values* for the energy and flux functions, namely $E' = -\eta v_f$, $\mathcal{F} = 32\eta^2 v_f^{10}/5$, and $\dot{F} = 96\eta v_f^{11}/(5\pi M^2)$, the SNR reduces to:

$$\rho(M, \eta, d; \theta, \bar{\phi}, \bar{\psi}, i) = \frac{M^{5/6} \eta^{1/2}}{d\pi^{2/3}} \mathcal{C}(\theta, \bar{\phi}, \bar{\psi}, i) \left[\frac{5}{6} \int_0^{F_{\text{cut}}} \frac{f^{-7/3}}{S_h(f)} df \right]^{1/2}, \quad (22)$$

Here F_{cut} is the frequency where the data analyst chooses to terminate the signal. The cutoff frequency is usually chosen to be the frequency of the waves at the last stable orbit of the binary (cf. Sec. III A) which depends on the total mass of the two stars and their spin magnitude. Note that the SNRs depend only on the combination $\mathcal{M} = M\eta^{3/5}$ – the chirp mass – and not on individual masses of the system. For a given total mass the SNR at a fixed distance (alternatively the span of the antenna at a fixed SNR) is the highest for binaries of equal masses (when $\eta = 1/4$) and reduces by the fraction $\sqrt{4\eta}$ for binaries of unequal masses. The SNR decreases inversely as the distance to the source and depends not only on the intrinsic parameters M , η and F_{cut} , but also on the relative orientations of the source and the antenna specified by the angles θ , $\bar{\phi}$, i , $\bar{\psi}$. We can compute the SNR for a source of RMS orientation by averaging the amplitude factor \mathcal{C} over all the angles. Performing the average over the angles leads to:

$$\langle F_+^2 \rangle_{\theta, \bar{\phi}, \bar{\psi}} = \langle F_\times^2 \rangle_{\theta, \bar{\phi}, \bar{\psi}} = \frac{1}{5}, \quad \langle \mathcal{C}^2 \rangle_{i, \theta, \bar{\phi}, \bar{\psi}} = \frac{4}{25}. \quad (23)$$

For an ideally oriented source, that is for a source that produces the highest SNR, $\mathcal{C} = 1$. Thus, the RMS and ideal SNRs, obtained by using $\mathcal{C} = 2/5$ and $\mathcal{C} = 1$, respectively, are given by [61]

$$\rho_{\text{RMS}} = \frac{\mathcal{M}^{5/6}}{d\pi^{2/3}} \left[\frac{2}{15} \int_0^{F_{\text{cut}}} \frac{f^{-7/3}}{S_h(f)} df \right]^{1/2}, \quad \rho_{\text{ideal}} = \frac{5}{2} \rho_{\text{RMS}}. \quad (24)$$

In Fig. 1 we have plotted the *RMS* SNR for the LIGO, VIRGO and GEO detectors, as a function of the spin magnitude and the total mass of the system. Clearly, systems with large spins in which the test mass is in prograde orbit produce the highest SNRs since their last stable orbit frequency is higher than those of retrograde orbits and they last longer. To capture such signals, however, one must know the phasing of the waves very well since the bodies spend a substantial fraction of their time in the detector band in the strongly non-linear regime of the evolution. We shall show later in this paper that there could be a significant drop in the SNR, and a corresponding drop in the number of candidate events that can be detected, while P-approximants lose little SNR and therefore capture almost all events.

III. GRAVITATIONAL BINDING ENERGY AND FLUX FUNCTIONS

We can see from Eqs. (8) and (9) that the phase of the gravitational wave depends both on the energy and flux functions of the binary system. In the test-mass case, that is when one of the masses is far smaller than the other ($4\eta \ll 1$) so that the dynamics is governed entirely by the Kerr geometry of the massive body, we have an exact expression for the energy $E(x)$, but only a series representation for the flux $F(x)$. In the comparable-mass

case, wherein one cannot neglect the perturbation caused by the companion, both functions are represented only by post-Newtonian expansion. The standard approximants for $E(v)$ and $\mathcal{F}(v)$ are simply their successive Taylor approximants E_{T_n} and \mathcal{F}_{T_n} , respectively. The gravitational wave signal constructed using these Taylor approximants are called T-approximant signals or waveforms are simply T-approximants.

It was shown in Ref [36] that the convergence properties of both the energy and flux functions can be improved by using Padé approximation of well-defined energy and flux functions. Damour, Iyer and Sathyaprakash followed a two-pronged approach to construct improved energy and flux functions [36]: Starting from the more basic energy-type and flux-type functions, $e(v)$ and $l(v)$, Ref. [36] constructs Padé-type approximants, say e_{P_n} , l_{P_n} , of the “basic” functions $e(v)$, $l(v)$. One can then compute the required energy and flux functions entering the phasing formula. The successive approximants $E[e_{P_n}]$ and $\mathcal{F}[e_{P_n}, l_{P_n}]$ have better convergence properties than their Taylor counterparts $E_{T_n}[e_{T_n}]$ and $\mathcal{F}_{T_n}[e_{T_n}, l_{T_n}]$.

In this study we will restrict ourselves to the test mass approximation and, therefore, employ the exact energy function. However, in the same approximation the flux function has been computed analytically only as a Taylor series although numerically the flux has been computed exactly. Since our aim is to draw conclusions on how effective P-approximants are in the comparable mass case, wherein one has only a Taylor expansion of the flux, we construct P-approximants of flux and compare it with the numerical results. The reasons for constructing a new flux function are the following: Firstly, it is well known, in the Schwarzschild case, that a simple pole exists at $r = 3M$ [23] in the expression for the flux. We might, therefore, expect that a similar pole exists in the Kerr case. A Taylor approximant of the flux function will never produce a pole while the equivalent Padé approximant, which is essentially a rational polynomial, will have a pole. Although it is well known that Padé approximants have the ability to model functions which are subject to singularities [48, 49] it is not guaranteed that the rational polynomial will reproduce the exact pole. Secondly, it is often possible to recover from the *divergence* [62] of a Taylor series by using Padé approximation. Again, one cannot be certain that the resulting Padé approximant, even when it converges, will be closer to being exact than any of the Taylor approximants, but experience with the test mass approximation in the Schwarzschild case render some optimism to this expectation.

We create a Padé approximation of a truncated power series of an analytic function containing n terms by equating it to a rational function such that the rational function when expanded as a power series and truncated to order n coincides with the original power series. More precisely, Padé approximation can be thought of as an operator P_M^N that acts on a polynomial $\sum_{k=0}^n a_k v^k$ to define a rational function:

$$P_M^N \left(\sum_{k=0}^n a_k v^k \right) = \frac{\sum_{k=0}^N A_k v^k}{1 + \sum_{k=1}^M B_k v^k}, \quad (25)$$

such that the number $N + M + 1$ of coefficients in the rational polynomial on the right hand side is the same as the number $n + 1$ of Taylor coefficients on the left hand side. By setting $N = M + \epsilon$ with $\epsilon = 0, 1$, we can define two types of Padé approximants: These are the super-diagonal, $P_M^{M+\epsilon}$, and sub-diagonal, $P_{M+\epsilon}^M$, approximants. Normally, the sub-diagonal approximants are preferred over super-diagonal approximants. This is because when $M = N + \epsilon$ the right hand side of Eq. (25) can be re-expanded as a continued fraction which have the property that as we go to each new order of the power series only one new coefficient needs to be calculated. Conversely, with the super-diagonal approximants, we would have to re-calculate all the A ’s and B ’s in the above equation as we go to higher orders in the Taylor expansion. This means that the sub-diagonal Padé approximants are more *stable* and if we see a trend of convergence in the coefficients the addition of a term is not likely to spoil this convergence. We refer the reader to Appendix A for a more summary of the properties of Padé approximations and how to find the diagonal Padé coefficients using continued fraction expansion.

A. The Orbital Energy.

In the case of both Schwarzschild and Kerr black holes we have an exact expression for the orbital energy of a test particle in a circular orbit around the parent black hole. For a black hole of mass M the energy E in terms of the dimensionless magnitude of velocity $v \equiv \sqrt{M}/r$, r being is the radial coordinate in the Boyer-Lindquist coordinates, takes the form [50]

$$E(v, q) = \eta \frac{1 - 2v^2 + qv^3}{\sqrt{1 - 3v^2 + 2qv^3}}. \quad (26)$$

where q is a dimensionless spin parameter given in terms of the spin angular momentum J of the black hole by $q \equiv J/M^2 \equiv a/M$, with a spin angular momentum per unit mass in the Kerr metric. It is actually the derivative of the orbital energy that appears in the phasing formula given by:

$$E'(v, q) = -v\eta \frac{1 - 6v^2 + 8qv^3 - 3q^2v^4}{(1 - 3v^2 + 2qv^3)^{3/2}}, \quad (27)$$

where a prime denotes a derivative with respect to the velocity parameter v .

For black holes with spin, the positions of the last stable circular orbit is a function of the spin parameter q . In order to find the position of the last stable circular orbit we take $E'(v, q) = 0$ which gives [50]:

$$r_{LSO}^{\pm}(q) = M \left[3 + z_2(q) \mp \sqrt{[3 - z_1(q)] [3 + z_1(q) + 2z_2(q)]} \right], \quad (28)$$

where

$$z_1(q) = 1 + (1 - q^2)^{\frac{1}{3}} \left[(1 + q)^{\frac{1}{3}} + (1 - q)^{\frac{1}{3}} \right] \quad (29)$$

$$z_2(q) = \sqrt{3q^2 + z_1^2}. \quad (30)$$

The $+$ ($-$) sign on r_{LSO} corresponds to prograde (retrograde) orbits. Now the position of the last unstable circular orbit or “photon ring” occurs where the energy function exhibits a pole. Thus, the photon orbit is found by solving a cubic equation. Of the three poles, the physically relevant pole is given by [50, 51]

$$r_{pr}^{\pm}(q) = 2M \left[1 + \cos \left[\frac{2}{3} \cos^{-1}(\mp q) \right] \right], \quad (31)$$

where once again the different signs define a prograde (retrograde) orbit. In the limit of $q \rightarrow 1$, both r_{LSO} and r_{pr} move towards the horizon of the black hole,

$$r_H^{\pm} = M \left(1 \pm \sqrt{1 - q^2} \right). \quad (32)$$

In the maximally rotating case of $q = 1$, we cannot distinguish between the last stable orbit and the light ring. This means, the greater the spin of the BH, the closer the particle can approach to it before beginning the plunge phase. On the other hand, in the limit $q \rightarrow -1$, the position of r_{LSO} moves outwards from the BH. Thus the particle begins its plunge much earlier than in the prograde case. Finally, for a particle in an orbit about a Schwarzschild black hole the above equations give the familiar position of $r = 6M$ for the LSO and $r = 3M$ for the photon ring.

B. The Flux Function

As discussed in the Introduction it has not been possible to derive an exact analytical expression for the flux of gravitational waves emitted by a binary system although analytic approximate expressions, and exact numerical results, have been computed. In the interesting case of two comparable masses in orbit around each other post-Newtonian methods have been used to derive an expression for the flux to quite a high order in the expansion parameter. However, since post-Newtonian theory is known to be poorly convergent, especially when the expansion parameter approaches unity, it has been suggested to employ in its place an equivalent rational polynomial, or Padé approximation, to the (modified) flux function. Since the purpose of this paper is to test the effectiveness of such an approximation we need a firm ground on which we can conduct our test.

In the case of a test mass in an equatorial orbit around a Kerr black hole numerical methods have been used to compute the flux to all post-Newtonian orders. This is, of course, valid only in the limit of vanishingly small mass of the test body as compared to the central object. However, all the relativistic corrections, including hereditary effects, such as the back scattering of gravitational waves off the curved background geometry, would be present in this computation. The deformation of the geometry due to the presence of the second body, or the back reaction of the waves on the motion of the test body, which would in turn affect the emission process, will not have been included in such a calculation. The deformation of the geometry, parametrized by the symmetric mass ratio of the system η , is important only a few orbits before the two objects merge. This should be expected from the fact that both in Newtonian and Einsteinian gravity it has been possible to construct an effective one-body formalism to describe the

dynamics of a binary and the dynamics derived within this formalism is expected to be valid close to the point when the two bodies plunge towards each other. Therefore, we expect that the deformation of the system will not bring about a major change in the analytic behaviour of the flux and lessons learnt in the test mass approximation will be applicable, albeit qualitatively, in the comparable mass case.

Thus, our strategy is to employ the test mass exact flux computed numerically together with the analytic expression for the energy function discussed in the previous Section. These two exact functions, together with the energy balance equation, can be used to construct an exact phasing formula for the inspiral signal. We shall also define an approximate phasing formula using the corresponding post-Newtonian expansions of the two functions. Our approximations at each post-Newtonian order will be one of two types: (1) The standard post-Newtonian or (2) the improved Padé approximation. In the next Section we will discuss how these approximations can be further improved and in the last Section we will measure the quantitative performance of the two approximations.

C. Post-Newtonian flux function

For a test-particle in a circular equatorial orbit the post-Newtonian expansion of the flux function has been calculated up to $\mathcal{O}(v^{11})$ in the case of a Schwarzschild BH [28], and to $\mathcal{O}(v^8)$ in the case of a Kerr BH [31, 32]. The general form of the flux function in both these cases is given by the expression

$$F_{T_n}(x; q) = F_N(x) \left[\sum_{k=0}^n a_k(q)x^k + \ln(x) \sum_{k=6}^n b_k(q)x^k + \mathcal{O}(x^{n+1}) \right]. \quad (33)$$

where the expansion is known to order $n = 8$ and 11 , in the Kerr and Schwarzschild cases, respectively, q is the dimensionless spin parameter introduced earlier and $F_N(x)$ is the dominant *Newtonian* flux function given by

$$F_N(x) = \frac{32}{5}\eta^2 x^{10}. \quad (34)$$

Here, x is the magnitude of the invariant velocity parameter observed at infinity which is related to the angular frequency Ω by $x = (M\Omega)^{1/3}$. The relation between the parameter x and the local linear speed v in Boyer-Lindquist coordinates is given by

$$x(v, q) = v [1 - qv^3 + q^2v^6]^{1/3}, \quad (35)$$

which reduces, in the Schwarzschild limit, to $x = v$. Note that this local linear velocity is related to the Boyer-Lindquist radial coordinate r by $v^2 = M/r$. The spin-dependent coefficients, $a_k(q)$, and the log-term coefficients, b_k , are given by [63],

$$\begin{aligned} a_0 = 1, \quad a_1 = 0, \quad a_2 = -\frac{1247}{336}, \quad a_3 = 4\pi - \frac{11q}{4}, \quad a_4 = -\frac{44711}{9072} + \frac{33q^2}{16}, \quad a_5 = -\frac{8191\pi}{672} - \frac{59q}{16} \\ a_6 = \frac{6643739519}{69854400} - \frac{1712\gamma}{105} + \frac{16\pi^2}{3} - \frac{3424 \ln 2}{105} - \frac{65\pi q}{6} + \frac{611q^2}{504}, \\ a_7 = -\frac{16285\pi}{504} + \frac{162035q}{3888} + \frac{65\pi q^2}{8} - \frac{71q^3}{24}, \\ a_8 = -\frac{323105549467}{3178375200} + \frac{232597\gamma}{4410} - \frac{1369\pi^2}{126} + \frac{39931 \ln 2}{294} - \frac{47385 \ln 3}{1568} - \frac{359\pi q}{14} + \frac{22667q^2}{4536} + \frac{17q^4}{16}, \\ b_6 = -\frac{1712}{105}, \quad b_7 = 0, \quad b_8 = \frac{232597}{4410}, \end{aligned} \quad (36)$$

where γ is Euler's number. For graphical purposes, it is more appropriate to deal with the Newton-normalized fluxes defined by

$$\widehat{F}_{T_n}(x) \equiv F_{T_n}(x)/F_N(x). \quad (37)$$

D. P-approximant of the flux function

We will now outline the method of calculation the P-approximant of the GW flux as proposed by DIS [36]. We notice from the form of the series expansion for the flux, Eq. (33), that we begin to encounter logarithmic terms at order x^6 and above. In general, series approximations of this form have slow convergence properties. In order to

prepare the series representation of the flux for creating the Padé approximation, it is convenient if we factor out the logarithmic terms. We can then write Eq. (33) as

$$\widehat{F}_{T_n}(x) = \left[1 + \ln \left(\frac{x}{x_{LSO}} \right) \sum_{k=6}^n l_k x^k \right] \left[\sum_{k=0}^n c_k x^k \right], \quad (38)$$

where the new coefficients c_k and l_k are functions of the old coefficients a_k and b_k . As in Ref. [36] the log-terms have been “normalized” using the value of the velocity parameter at the LSO; this helps in reducing the importance of the log-terms. Factoring out the logarithmic terms aids in constructing the rational polynomial, or the Padé approximation, of the reminder. Moreover, since we expect the flux to have a pole at the location of the light ring it is best to factor out the expected pole so that the reminder has good analytical properties. To this end we create the factored flux function, $f_{T_n}(x)$ by the operation

$$f_{T_n} \equiv \left(1 - \frac{x}{x_{pole}} \right) \widehat{F}_{T_n}. \quad (39)$$

Factoring out the pole also helps to alleviate the problem arising from the absence of the linear term in the PN expansion of the flux. (Note that $a_1 = 0$ in both the Schwarzschild and Kerr cases.) We can see from Appendix A that in the absence of such a term the continued fraction form of the Padé approximation, the so-called diagonal Padé approximant, would lead either to zero or infinite Padé coefficients. The above operation rectifies this problem by introducing a linear term into the Taylor series for the flux. If we write the expression in full we obtain

$$f_{T_n}(x) = \left[1 + \ln \left(\frac{x}{x_{LSO}} \right) \sum_{k=6}^n l_k x^k \right] \left[\sum_{k=0}^n f_k x^k \right], \quad (40)$$

where $f_0 = c_0$ and $f_k = c_k - c_{k-1}/x_{pole}$, $k = 1, \dots, n$.

We can now construct a new flux function by using the Padé approximant of the factored flux given above. Indeed, we can construct two variants of the new flux: The first one is what we call the *Direct* or D-Padé approximant, which is obtained by directly starting from the flux function $f(v)$ in Eq. (40) and constructing the equivalent rational polynomial. This is the approach followed in DIS. An alternative approach to this is motivated by the fact that in the gravitational wave phasing formula the flux appears in the denominator. Thus, instead of constructing the Padé approximant of the flux function one could first construct the polynomial expansion of the inverse of the flux function and construct the Padé approximant of the resulting polynomial. We call the approximant constructed this way as *Inverse*- or I-Padé approximant because it is obtained from the Taylor expansion of the *inverse* of the flux function $f(v)$ in Eq. (40). Thus, our two improved versions of the flux are defined as follows: The Direct Padé approximant is defined by

$$f_{DP_n}(v) \equiv \left[1 + \ln \left(\frac{x}{x_{LSO}} \right) \sum_{k=6}^n l_k x^k \right] P_{m+\epsilon}^m \left[\sum_{k=0}^n f_k x^k \right], \quad (41)$$

where $P_{m+\epsilon}^m$ is the diagonal or sub-diagonal Padé approximant, $n = 2m + \epsilon$, with $\epsilon = 0$ or 1 , depending on whether n is even or odd. The Inverse Padé approximant of flux is defined by

$$f_{IP_n}(v) \equiv \left[1 - \ln \left(\frac{x}{x_{LSO}} \right) \sum_{k=6}^n l_k x^k \right] P_{m+\epsilon}^m \left[\sum_{k=0}^n d_k x^k \right], \quad (42)$$

where the coefficients d_k in the Taylor expansion are defined by

$$\sum_{k=0}^n d_k x^k \equiv \left(\sum_{k=0}^n f_k x^k \right)^{-1}. \quad (43)$$

One finds d_k by first expanding the RHS in a binomial series and then identifying the coefficients of the various terms with those on the LHS.

Having constructed the rational polynomials equivalent to a given truncated Taylor series of the modified flux function we can return to the original flux function that appears in the phasing formula. We shall call the flux function so constructed as *P-approximant*, and not just Padé approximant to remind ourselves that the new flux has been obtained by improving the convergence properties in two steps (i.e., definition of a new flux function and the

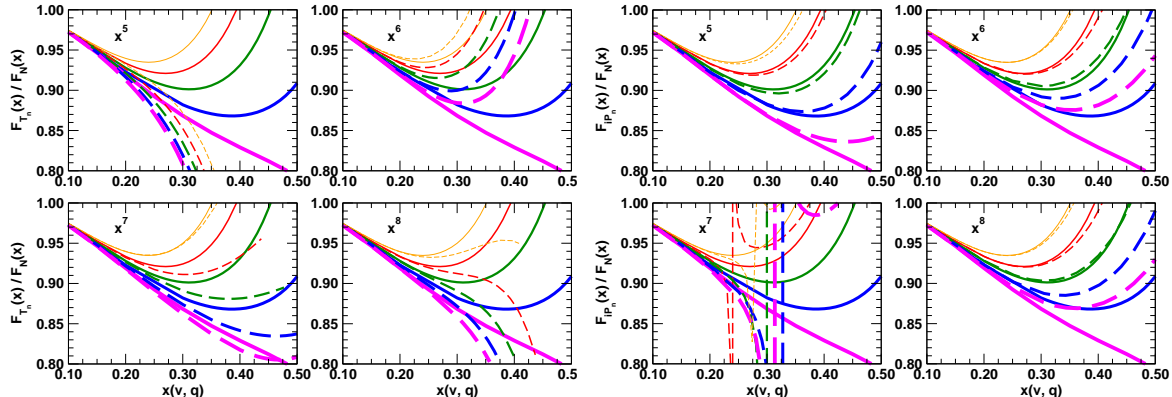


FIG. 2: The convergence of the Newton-normalized T-approximants (left panels) and Inverse P-approximants (right panels) to GW flux at post-Newtonian orders $\mathcal{O}(x^5)$ to $\mathcal{O}(x^8)$, for a test particle in prograde orbit around a Kerr black hole. The solid lines represent the exact numerical fluxes with thicker lines corresponding to larger spin magnitudes, $q = \{0, 0.25, 0.50, 0.75, 0.95\}$, respectively. The correspondingly thickened dashed lines represent the Taylor- and P-approximants.

construction of its rational polynomial) and not just a direct application of Padé approximation. Thus, we define the *Direct P-approximant* of flux as

$$\widehat{F}_{DP_n}(v) = \left(1 - \frac{x}{x_{pole}}\right)^{-1} f_{DP_n}(v), \quad (44)$$

and *Inverse P-approximant* as,

$$\widehat{F}_{IP_n}(v) = \left[\left(1 - \frac{x}{x_{pole}}\right) f_{IP_n}(v)\right]^{-1}. \quad (45)$$

Detailed investigation shows that Inverse P-approximants of flux, namely \widehat{F}_{IP_n} , have better convergence properties than Direct P-approximants. We shall therefore use only \widehat{F}_{IP_n} in all our investigations in the rest of this paper.

E. Convergence of the Kerr flux function

In this Section we will look at the convergence properties of the post-Newtonian series representations and the improved P-approximants of the flux function discussed in the last Section. To this end we shall employ all the post-Newtonian orders up to which the Taylor expansions have been worked out in the Kerr case. We shall investigate the convergence of the approximants in the case of a test particle (i.e., $\eta \rightarrow 0$ limit) either co-rotating (i.e., $q > 0$, *prograde orbits*) or counter-rotating (i.e., $q < 0$, *retrograde orbits*), with respect to a central black hole whose spin parameter q takes nine values over the full range from $(-1, 1)$. In this Section we shall make a graphical comparison of the analytical and numerical fluxes and assess the performance of the flux with respect to variation in the spin-parameter values at increasingly higher post-Newtonian orders. We will find that neither the post-Newtonian series nor their improved versions fit the numerical flux exactly when the parameters are chosen to be the same for analytical fluxes as the numerical flux. However, the P-approximant fluxes agree with the numerical fluxes quite closely when their spin values are slightly mis-matched with the true values of the numerical fluxes. The post-Newtonian approximants do show this improved behaviour, albeit not to the extent of P-approximants. Thus, we can expect the P-approximants to define better signal models than post-Newtonian approximants with regard to both faithfulness and effectualness.

1. Prograde Orbits, $q \geq 0$

The numerical fluxes have been computed exactly [52], but in the test mass approximation, at a set of test values of the spin parameter q . For prograde orbits the flux has been computed at $q = \{0.25, 0.50, 0.75, 0.95\}$. For the sake of completeness, we shall also include in our comparison the numerical flux for a particle in orbit about a Schwarzschild BH, i.e. $q = 0$ [28]. In Fig. 2 we have plotted the Newton-Normalized numerical fluxes alongside analytical fluxes for

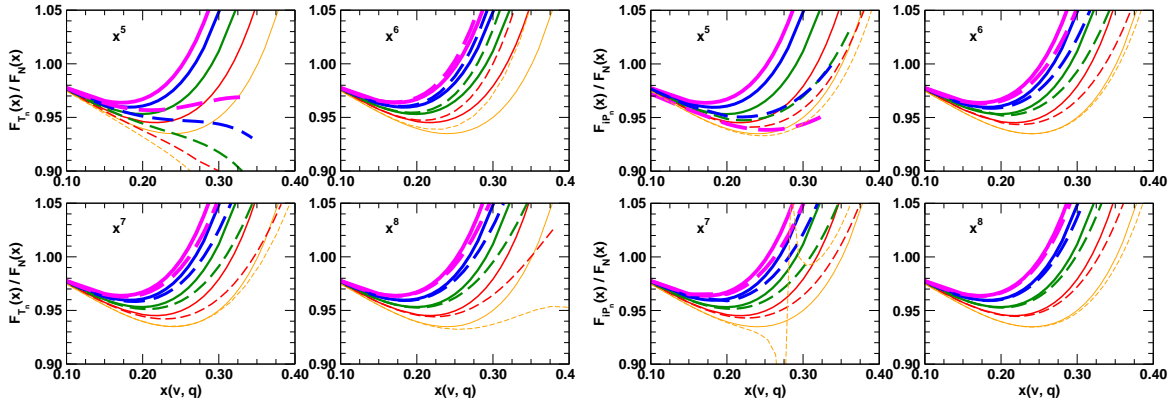


FIG. 3: The convergence of the Newton-normalized T-approximants (left panels) and Inverse P-approximants (right panels) to GW flux at post-Newtonian orders $\mathcal{O}(x^5)$ to $\mathcal{O}(x^8)$, for a test particle in retrograde orbit around a Kerr black hole. The solid lines represent the exact numerical fluxes with thicker lines corresponding to larger spin magnitudes, $q = \{0, -0.25, -0.50, -0.75, -0.95\}$, respectively. The correspondingly thickened dashed lines represent the Taylor- and P-approximants.

both the truncated Taylor approximants (four panels on the left) and (Inverse) P-approximants (four panels on the right). For each approximant, we consider four post-Newtonian orders at $\{x^5, x^6, x^7, x^8\}$ and five spin values. The solid lines with increasing thickness correspond to the exact numerical fluxes at progressively larger values of the spin parameter starting at $q = 0$, (thinnest line) and ending at $q = 0.95$ (thickest line). The corresponding dashed lines represent the analytical approximant to the GW flux.

Let us first concentrate on the post-Newtonian fluxes: We notice immediately that at all values of q , and large values of x , the 2.5 post-Newtonian approximant $\mathcal{O}(x^5)$ is highly divergent. Indeed, this order has been known to exhibit improper behaviour in the Schwarzschild case and continues to be so for prograde orbits in Kerr. The situation improves at $\mathcal{O}(x^6)$, but begins to worsen again at $\mathcal{O}(x^7)$, becoming highly divergent at $\mathcal{O}(x^8)$. The plots serve to illustrate the principal problem with the PN expansion: Going to higher orders of the approximation does not necessarily correspond to a better accuracy.

The sequence of panels on the right-hand-side of Fig. 2 demonstrates that the P-approximant flux has improved convergence properties over the post-Newtonian flux for the same range of post-Newtonian orders and spins. The extreme divergence which the post-Newtonian flux exhibited at $\mathcal{O}(x^5)$ and $\mathcal{O}(x^8)$ has been cured. Let us note, however, that sometimes the rational polynomial approximation of a Taylor series can produce spurious poles in the region of interest [64]. An example of this can be seen at $\mathcal{O}(x^7)$ which shows a spurious pole at every value of q . The main factor that stands out in the right panels of Fig. 2 is the following: The P-approximant fluxes display the same characteristic shape as the numerical fluxes although they don't agree with the exact flux at higher values of the parameter x .

In the case of prograde orbits the P-approximants graphically display a closer convergence to the numerical fluxes: While being better than the Taylor approximation, they are still not as good as we would like. However, we must remember that what is more important is how the phasing of the waveforms defined by the two approximants match with that defined by the exact flux, rather than a simple graphical agreement of the flux. The graphical display is useful as it gives us a rough idea on any improvement in performance of a particular model. But as the noise of the interferometer weights the inner-product between templates, it may emphasize a particular range of frequency of the waveform more than the other. It may turn out that the divergent region of a particular model is outside the detector bandwidth for most masses. In such cases the approximant may work well in spite of the divergences or poles. We shall return to this question in Sec. IV when we consider the matching of waveforms.

2. Retrograde Orbits, $q < 0$

We now focus on the GW flux from a test-mass counter-rotating with respect to the black hole. We will again use a similar set of spin values, i.e. $q = \{-0.25, -0.50, -0.75, -0.95\}$, as well as the Schwarzschild flux for comparative purposes. In Fig. 3, left panels, we plot the Taylor approximant flux for retrograde orbits. The solid lines in the figure correspond to the exact numerical fluxes with thicker lines corresponding to smaller spin values $q = 0, -0.25, -0.50, -0.75, \text{ and } -0.95$, respectively. The correspondingly thickened dashed lines represent the Taylor

TABLE I: The “best-fit” value of the spin parameter, q , for T and P-approximant fluxes for $q = -0.95$ to $q = 0.95$. For the Schwarzschild case we have an absolute error of 0.11 in the case of T-approximant and -0.08 in the case of P-approximant.

Spin Magnitude	-0.95	-0.75	-0.50	-0.25	0.25	0.50	0.75	0.95
q_T	-0.90	-0.68	-0.42	-0.13	0.35	0.62	0.89	0.99
q_P	-0.99	-0.81	-0.60	-0.33	0.21	0.55	0.90	0.99
σ_{q_T}	5.3%	9.3%	16%	48%	40%	24%	19%	4.2%
σ_{q_P}	4.2%	8.0%	20%	32%	16%	10%	20%	4.2%

series approximation to the GW flux with the same spin magnitude as the numerical flux. The right panels are the same except that in place of Taylor approximant fluxes we plot the Inverse P-approximant fluxes.

The first thing we notice is that just as in the case of prograde motion the $\mathcal{O}(x^5)$ and $\mathcal{O}(x^8)$ approximants are again highly divergent although at $\mathcal{O}(x^8)$, the convergence of the PN approximation improves as we go to larger negative spins. This is not entirely surprising: As we go to larger counter-rotating spins the higher order Taylor expansion coefficients become smaller and the non-linear general relativistic corrections are not as important as in the case of prograde orbits. Moreover, the position of the LSO moves outwards from the BH as q becomes more negative. At $q = -0.25$, the LSO is at $r_{LSO} \sim 6.8M$. This corresponds to $x_{LSO} \sim 0.38$. At $q = -0.95$ the LSO has moved outwards to $r_{LSO} \sim 9M$, corresponding to $x_{LSO} \sim 0.33$. If we compare this to the equivalent spins in the prograde case we find that for $q = 0.25$, $r_{LSO} \sim 5M$ and $x_{LSO} \sim 0.44$. At $q = 0.95$, $r_{LSO} \sim 2M$ and $x_{LSO} \sim 0.7$. In other words, retrograde orbits are weakly bounded orbits in comparison to prograde orbits and experience smaller relativistic corrections. Recalling that gravitational wave luminosity $\propto x^{10}$, retrograde flux for $q = -0.95$ at LSO is smaller by a factor $(0.70/0.38)^{10} \simeq 500$ compared to prograde flux for $q = 0.95$ at LSO. Consequently, the PN approximation seems to work well in the retrograde case.

In the case of retrograde orbits P-approximants provide, at order $\mathcal{O}(x^5)$, only a marginal improvement over T-approximants. This is in sharp contrast to the prograde case where the improvement was excellent. At orders $\mathcal{O}(x^6)$ and $\mathcal{O}(x^8)$ are again quite good, with no poles at $\mathcal{O}(x^7)$ for most spin values. While there seems to be a less obvious benefit in using the P-approximant flux in the retrograde case, it is again important to note that the P-approximants show the same general behaviour as the exact flux in the retrograde case too and can therefore be expected to match the true general relativistic signal more closely.

F. Improving the performance of the Taylor- and P-approximants

In the last two Sections we noted how the P-approximant sequence seems to have a character similar to the sequence given by the numerical computations although the two do not agree perfectly. This suggests that if the value of the spin parameter used in the T- or P-approximant fluxes is varied relative to the true value of the spin parameter in the exact flux, we should be able to obtain a better fit to the numerical fluxes. While we will initially do this graphically, we remind the reader that this exercise is purely demonstrative. As the fluxes are Newton-normalized, it is difficult to say in what region of the velocity we should attempt to make the best fit. Added to this is the fact that when matching templates we should take the weighting of the PSD into account. However, if the approximant fluxes agree graphically well with the numerical fluxes then it would mean that we should be able to match the T- or P-approximant flux with the numerical result without introducing any new parameters. To examine how best mis-matching spins might work we will focus on one of the post-Newtonian orders, say $\mathcal{O}(x^6)$, the order at which the T-approximants work well and P-approximants have no spurious poles.

In Fig. 4, left panel, we have plotted the best-fit for the T-approximant flux for various values of the spin magnitude from $q = -0.95$ (top most curve) to $q = 0.95$ (bottom most curve). For each spin magnitude we have fitted the T-approximant with the numerical result as best as possible by varying the spin-magnitude of the approximant. In best fitting the numerical flux we incurred errors (defined as $\sigma_q \equiv 1 - q_{\text{fitted}}/q_{\text{exact}}$) in the spin magnitude of the approximant relative to the exact case. These are listed in Table I. Although the errors decrease as we approach the extreme prograde flux, we can see from the figure that the fit is not very good for the Taylor approximant for $q \geq 0$. Schwarzschild case.

We have plotted the best-fit results for the P-approximant in right panel of Fig. 4. We can observe that while the fit is not as good as the PN flux in the extreme retrograde case, it gets superior as we move towards the extreme prograde flux. In fact, the P-approximant best-fits work extremely well up to a spin of $q = 0.5$. It also works well at $q = 0.75$, but only at low values of the parameter x . For $q = 0.95$ we did not obtain a good fit without introducing a

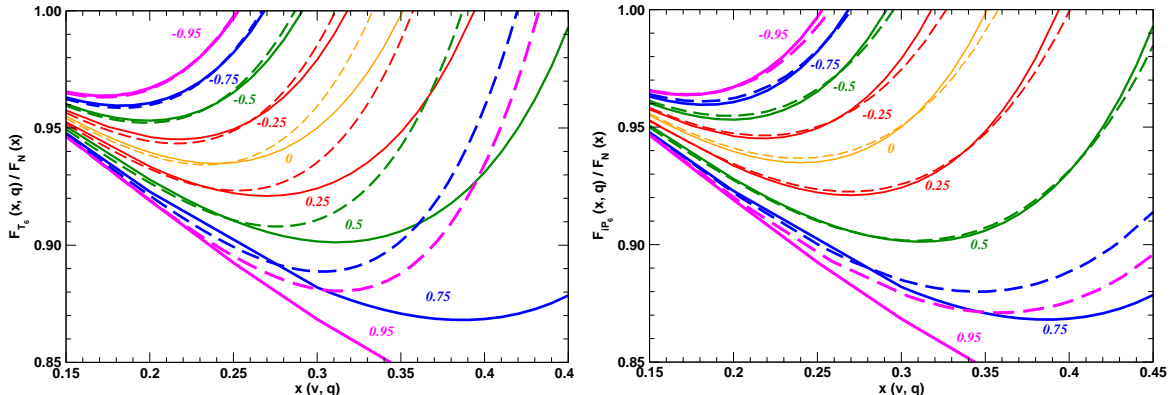


FIG. 4: A best-fit for T-approximant (left) and P-approximant (right) fluxes by varying the spin parameter q at the $\mathcal{O}(x^6)$ level for $q = -0.95$ (top most curve) through to $q = 0.95$ (bottom most curve). Once again, the solid lines represent numerical fluxes and the broken lines represent the approximated fluxes.

new parameter. It is clear that there is an advantage in using the P-approximant flux. However, we will have to wait until we calculate the fitting factors between templates to see just how important this advantage is.

Let us conclude this Section by noting that when approximate fluxes, both T- and P-approximants, best fit the exact numerical flux, errors in relative spin magnitude are large at low values of spins, i.e. several 10's of percents for $|q| \leq 0.50$, while the errors are low at large spin magnitudes, i.e. a few percents for $|q| \geq 0.75$. We will see that this will exactly be the case even when we compute the best overlap of the approximate signal with the exact signal.

IV. EFFECTUALNESS AND FAITHFULNESS OF T- AND P-APPROXIMANTS

In Sec. II we have seen that the phase of the GW depends on the evolution of the binary's binding energy and gravitational wave flux functions. As the energy is known exactly for a test-particle in circular orbit about a Kerr black hole it is important to compute the flux to sufficiently high accuracy so that we can match the phasing of the exact waves to a good precision. Investigations of the PN approximation showed that while T-approximants have bad convergence properties P-approximants improved the convergence of the flux. We also found that we could use the spin parameter q as a free parameter in order to obtain a better matching of the flux. By best fitting the spin parameter, we were able to graphically achieve a closer fit to the numerical fluxes. Equipped with the new, improved, P-approximant we now move onto explore how well a waveform based on it matches the phasing of the exact waves. We shall address the performance of the approximants in extracting the exact waveform in two ways: The *effectualness* of the templates measured in terms of the maximum overlap they can achieve with the exact waveform when the parameters of the approximant are varied in order to achieve a good match. The *faithfulness* of the approximant templates measured in terms of the systematic errors in the estimation of parameters while detecting exact waveforms.

A. Overlaps and fitting factor

We can employ the results of matched filtering, and its geometrical interpretation, to assess how well our approximant waveforms match the exact waveform. The geometrical theory of signal analysis [54, 55] can be summarized as follows: The set of all detector outputs, each lasting for a duration T , and sampled at a rate f_s , and consisting of $N = f_s T$ samples, can be thought of as a linear vector space. Parametrized signals, such as a binary inspiral waveform that depends on the two masses of the component stars and their spins, are also vectors in the vector space of all detector outputs. However, the set of all waveforms do not form a vector space although they do form a manifold with the parameters serving as coordinators.

Matched filtering technique, which is the most effective technique to capture signals of known phase evolution, can be used to define a metric on such a manifold. The metric and the associated scalar product allows us to compute the distance between any two signal vectors that are parametrized in the same way. The scalar product is the same as that introduced in Eq. (20). If we have two different families of waveforms, for example T- and P-approximants, parametrized similarly then each family lives on a distinct manifold. The distance between two vectors with exactly

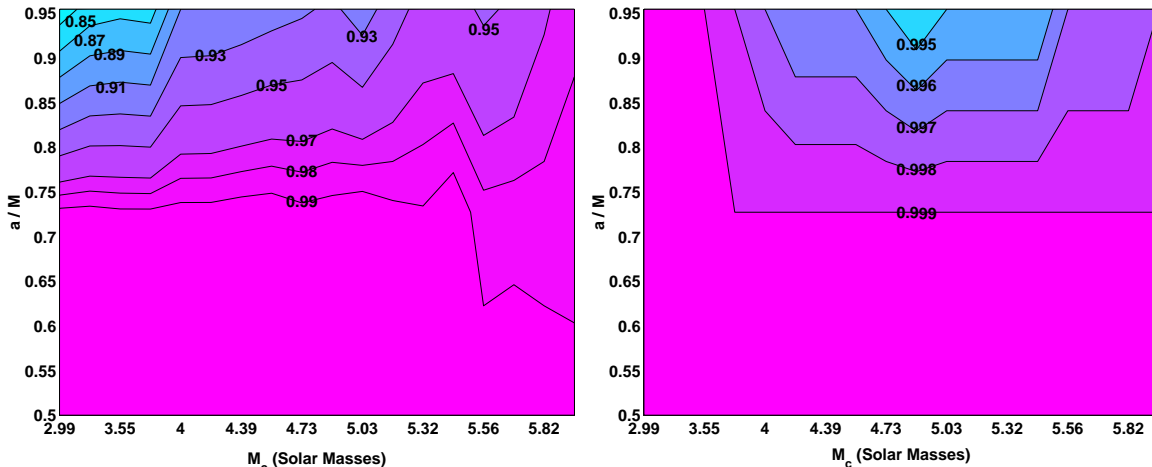


FIG. 5: The maximized prograde overlaps for T-approximant (left) and P-approximant (right) templates at the x^8 approximation. Each system consists of a $1.4 M_\odot$ NS inspiralling into a central BH of mass ranging from 10 - $50 M_\odot$. The figure covers prograde Kerr from $q = 0.5$ onwards, as fitting factors of > 0.99 are achieved for all lower spins.

the same parameters but belonging to different families is, in general, not zero. Although the scalar product can be computed between any two vectors in the space it is only in the case of two similarly parameterized signal vectors does the scalar product represent the distance between the vectors. This is because the coordinates, that is the parameters, don't have any meaning for vectors that don't live on the manifold. By calculating the scalar product between two normalized vectors, that is vectors whose scalar product with themselves is unity, we can see how well they match. For two normalized waveforms, or signal vectors, the scalar product returns the cosine of the angle between them and is normally referred to as the *overlap*, denoted by O . Given two waveforms h and g , not necessarily belonging to the same family of approximants, their overlap is defined as

$$O \equiv \frac{\langle h | g \rangle}{\sqrt{\langle h | h \rangle \langle g | g \rangle}}, \quad (46)$$

where, the inner-product between two real functions $h(t)$ and $g(t)$ is defined by Eq. (20). For detection of signals what is more important is the *fitting factor* FF : As each template is a function of the intrinsic parameters λ^μ , the fitting factor is defined as the maximum overlap obtained by varying the parameters of the template (or the approximate waveform) relative to the exact waveform:

$$FF = \max_{\lambda^\mu} O(\lambda^\mu). \quad (47)$$

If two waveforms are a perfect match then their overlap is unity. As the waveforms begin to differ, their overlap differs from 1 and the value of the overlap is a measure of how similar the two waveforms are and how useful one waveform is in extracting the other waveform buried in noise. Now the GW from a binary is determined by a number of parameters: The two masses, spins, eccentricity and the orientation of the angular momentum at some initial time. These parameters essentially determine the dynamics of the system and are called *intrinsic* parameters [55]. The observation of such a system introduces five other parameters: These are the instant t_0 of coalescence (or the time at which the orbital frequency reaches a certain value) and the phase ϕ_0 of the system at that instant, the angular position of the system in the sky, the distance of the binary (or, equivalently, the amplitude of gravitational waves at Earth) and the polarisation angle (or, equivalently, the ratio of h_+ and h_\times). These are called the *extrinsic* parameters [55] and do not play any role in the dynamics of the system. For a signal that lasts only for a few mins, as would be the case for systems expected to be observed in a ground-based interferometer, the direction and the polarisation angle cannot be measured in a single interferometer and the distance is only an amplitude parameter. Thus the templates are only needed for parameters t_0 and ϕ_0 . In the case of circular equatorial orbits of a test mass around a central black hole, the wave is parameterized by the $(t_0, \Phi_0, M, \eta, q)$.

In order to improve the detection probability, we would like to maximize over as many of the parameters as possible. Maximization over t_0 is achieved by simply computing the correlation of the template with the data in the frequency domain followed by the inverse Fourier transform. This yields the correlation of the signal with the data for all time-lags. However, one has to worry about circulation correlation effects, and the consequent corruption of the

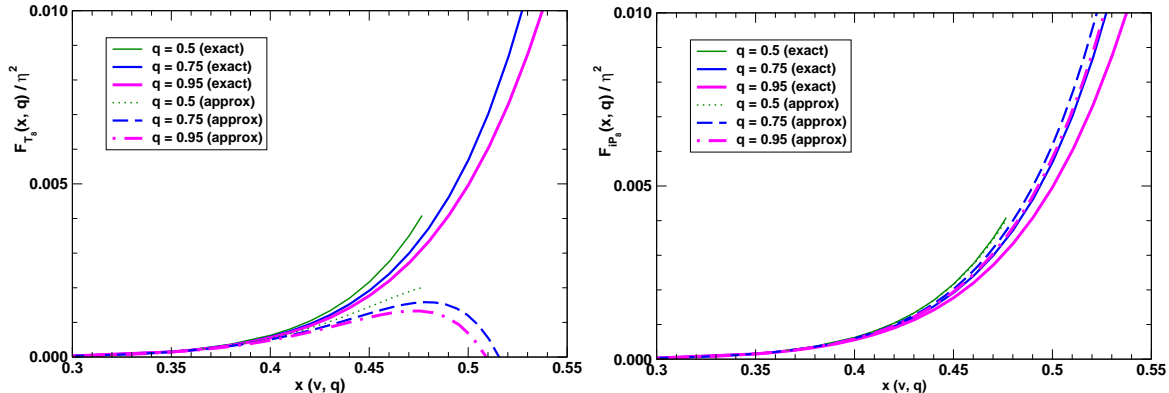


FIG. 6: The 4-PN T-approximant (left) and P-approximant (right) analytical flux function for spins of $q = 0.5, 0.75$ and 0.95 against the numerical fluxes for the same spin values. We can see that, beyond $q = 0.5$, the T-approximant flux goes to zero before the LSO is reached. This happens sooner, the higher the spin value we go to. This is not a problem for the P-approximant flux.

correlation when the template gets split at the boundaries of the sample sets, but these are easily handled by padding the template with sufficiently large number of zeroes before performing the Fourier transform.

It was pointed out by Schutz [12, 57] that the maximum of the correlation C of data with a template over Φ_0 can be computed using just two templates – an *in-phase* and a *quadrature-phase* template. In other words, generate two orthonormalized templates with phase $\Phi_0 = 0$ and $\Phi_0 = \pi/2$. The maximized overlap is then given by

$$\max_{\Phi_0} C = \sqrt{C_0^2 + C_{\pi/2}^2}, \quad (48)$$

where $C = \langle h^A(\Phi_0) | h^X \rangle$, $C_0 = \langle h^A(\Phi_0 = 0) | h^X \rangle$ and $C_{\pi/2} = \langle h^A(\Phi_0 = \pi/2) | h^X \rangle$. Here, h^X denotes some normalized “exact” waveform. However, numerically, this procedure does not fully orthogonalize the two templates. For this reason we specifically orthonormalize the two waveforms. Using two un-normalized waveforms $\tilde{h}_0 = \tilde{h}(\Phi_0 = 0)$ and $\tilde{h}_{\pi/2} = \tilde{h}(\Phi_0 = \pi/2)$, we generate two orthonormalized waveforms according to

$$\tilde{H}_0 = \frac{\tilde{h}_0}{|\tilde{h}_0|}, \quad \tilde{H}_{\pi/2} = \frac{\tilde{h}_{\pi/2} - \langle h_{\pi/2} | H_0 \rangle \tilde{H}_0}{|\tilde{h}_{\pi/2} - \langle h_{\pi/2} | H_0 \rangle \tilde{H}_0|}. \quad (49)$$

Alternatively, one could define the quadrature-phase template using $\tilde{H}_{\pi/2} \equiv i\tilde{H}_0$, which is explicitly orthogonal to the in-phase template. The (square of the) maximum of the overlap over Φ_0 is given by the sum-of-squares of the correlation with the in-phase and quadrature-phase templates:

$$\max_{\Phi_0} \langle C \rangle = \sqrt{\langle H_0 | h^X \rangle^2 + \langle H_{\pi/2} | h^X \rangle^2}. \quad (50)$$

Thus, the correlation can be easily maximized over the unknown time-of-arrival and the constant phase of the templates. However, we can also maximize over all other parameters using a grid of templates.

In this paper, as we are working in the test-mass approximation, we assume that our system is composed of objects with a small mass ratio. For concreteness we assume that the system comprises a $1.4M_\odot$ NS inspiralling into a central BH of varying spin magnitude and mass. Beginning with a central BH of $10M_\odot$, we work our way upward to a $50M_\odot$ BH. In terms of the symmetric mass ratio, this gives us a range of test systems from $\eta = 0.027$ for the heaviest binary in our list [i.e. $(50-1.4)M_\odot$ system] to $\eta = 0.11$ [i.e., $(10-1.4)M_\odot$ system]. We will also look at the limiting case of a $10-10M_\odot$ equal-mass system. Strictly speaking, the formulas for energy and flux functions used in this study are not applicable to the comparable mass case since we have neglected the finite mass correction terms in these quantities. However, the results of such a study should give us an indication of how strong are the relativistic corrections, as opposed to finite-mass corrections, in the case of comparable masses. In all cases we vary the spin magnitude of the central BH from $q = -0.95$ to 0.95 .

In the next two sub-sections, we will focus respectively on prograde and retrograde systems. As well as presenting the results for the fitting factors achieved, we will also focus on the problem of parameter extraction using templates constructed from the Taylor- and P-approximants. Since the main focus in this study is test-mass approximation we

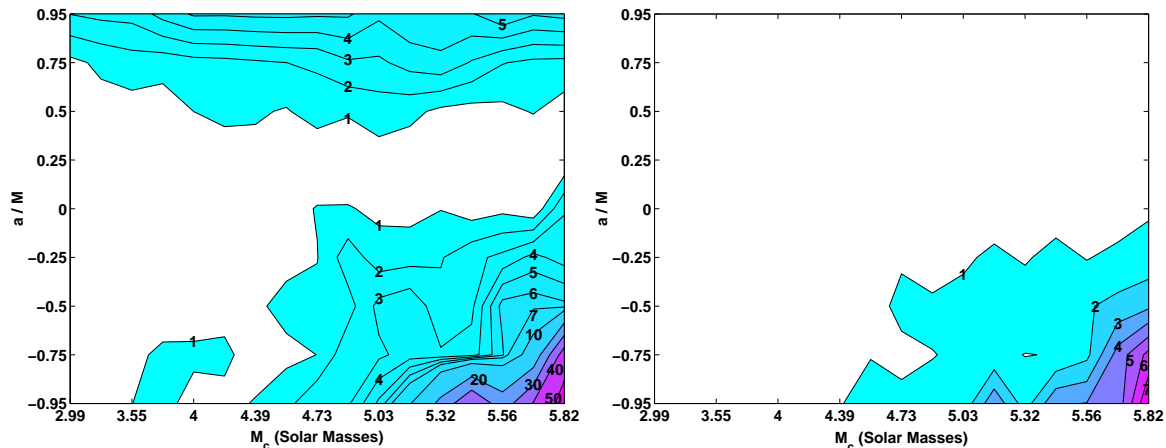


FIG. 7: The percentage error in the estimation of the chirp-mass, \mathcal{M}_c , for T-approximant (left) and P-approximant (right) templates at the x^8 approximation. The values of \mathcal{M}_c correspond to a $1.4 M_\odot$ NS inspiralling into a central BH of mass ranging from 10 - $50 M_\odot$. The figure covers retrograde Kerr, Schwarzschild and prograde Kerr systems.

shall be interested in only one of the mass parameters and consider errors in estimating the chirp-mass $\mathcal{M} = m\eta^{3/5}$ in addition to the spin magnitude of the central BH. In view of economy we shall only present the results for the highest PN order available, namely $\mathcal{O}(x^8)$ order. In all cases our fiducial *exact* signal h^X will be that obtained by using the exact expression for the energy in Eq. (26) and the exact numerical fluxes generated using black hole perturbation theory [52], and the template will be the approximate waveform constructed using the exact expression for the energy, as before, and an approximate expression for the flux, either the T-approximant flux, the corresponding template denoted h_T , or the P-approximant flux, the corresponding template denoted h_P .

B. Prograde Orbits – Effectualness

In the first instance, we maximized the overlap only over t_0 and Φ_0 , while holding all other parameters of the signal and the templates the same. The overlaps so obtained were not good enough. In the case of T-approximant templates the overlaps at $q = 0.25$ were in the range $0.6 \leq FF \leq 0.8$, depending on the PN order. By $q = 0.95$ they had fallen to $0.3 \leq FF \leq 0.5$. The P-approximants actually fared much worse in this case. At $q = 0.25$ the fitting factors lay between $0.25 \leq FF \leq 0.65$, while at $q = 0.95$, none of the fitting factors achieved was > 0.4 .

It is clear that maximizing over extrinsic parameters is not adequate: When we maximize over all other parameters, overlaps improve significantly as compared to the unmaximized overlaps. For T-approximants – Fig. 5, left panel – maximizing over all parameters gives fitting factors of $FF \geq 0.98$ at all mass ranges for the test-mass systems up to a spin of $q = 0.75$. Between 0.75 and $q = 0.95$, the T-approximant templates begin to perform badly and the fitting factors drop to $FF \sim 0.82$. For the equal-mass case – Fig. 9 – the templates once again achieve fitting factors of $FF \geq 0.99$ up to a spin of $q = 0.75$, but fall off at higher spin magnitudes achieving a fitting factor of ~ 0.98 at $q = 0.95$. We should point out that these results do not properly convey just how bad the 4-PN T-approximant template actually performs. In the left hand panel of Fig.6, we plot the PN approximation for the flux function against the numerical fluxes at spins of $q = 0.5, 0.75$ and 0.95 . We can see that the flux function at $q = 0.75$ and 0.95 become negative long before the LSO is reached. This means that as we go to higher and higher spins, we can model less and less of the waveform. For $q \leq 0.6$ we can model the waveform up to the LSO. However, for $q > 0.6$ this we have to stop the waveform generation at a cutoff velocity of $x_{cut} \approx 0.5$. At $q = 0.75$ we model approximately 80% of the waveform, while at $q = 0.95$, this reduces to 44%. Thus, T-approximants have to be prematurely terminated well before the LSO is reached. In the process of maximization of the overlap we systematically find that exact waveforms corresponding to a given total mass are maximized by T-approximant templates of significantly *smaller* masses. The reason for this is that smaller mass templates will have a longer duration (and therefore make up for the loss in overlap due to premature termination of the waveform) and thereby achieve a better overlap with the exact waveform.

Therefore, the fitting factors beyond $q = 0.75$ completely overestimate the performance of the T-approximant template.

If we now focus on the right hand panel of Fig.6, we see the true power of the P-approximant templates. The 4-PN template suffers none of the divergences that effect the T-approximants. We therefore generate all templates up to

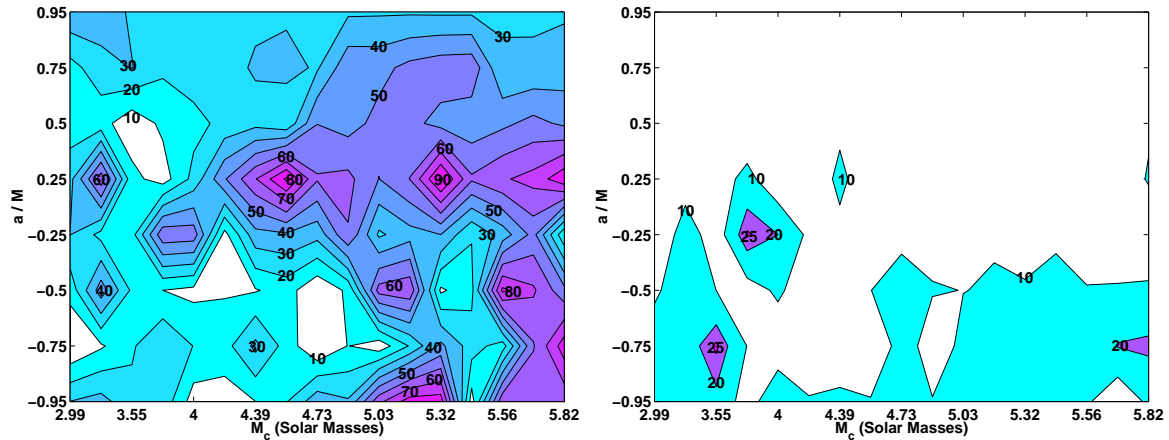


FIG. 8: The percentage error in the estimation of the spin parameter, q , for T-approximant (left) and P-approximant (right) templates at the x^8 approximation. The values of M_c correspond to a $1.4 M_\odot$ NS inspiralling into a central BH of mass ranging from 10 - $50 M_\odot$. The figure covers retrograde and prograde Kerr systems.

the LSO or 2 kHz, whichever is reached first. We can see from the right panel of Fig. 5 that the P-approximant templates achieve fitting factors of > 0.99 at all spin values. For the equal-mass case – Fig. 9 – the P-approximant templates achieve fitting factors of $FF \geq 0.995$ at all mass and spin levels. This demonstrates that in the case of prograde orbits, the P-approximant templates are clearly more robust, even at high spin magnitudes of $q = 0.95$.

C. Prograde Orbits – Faithfulness

Gravitational wave observations of the inspiral signal are expected to result in very precise measurements of the signal parameters. Indeed, it has been shown [53] that the chirp mass can be measured to a relative accuracy of 0.02% and 0.16% respectively for systems comprising $(10, 1.4)M_\odot$ and $(10, 10)M_\odot$ objects when the correlations between the spin magnitude and masses is neglected and to an accuracy of 0.19% and 1.42% for the same systems when the correlations are included. Such accurate estimation of parameters will aid in high precision tests of general relativity. When we use approximate templates the question naturally arises if the *bias* in the estimation of parameters [65] is smaller than the accuracy with which the parameters can be determined. This is what we shall consider next.

While the T-approximant templates performed well up to $q = 0.75$, a clear indication of how good they truly are comes from the bias in parameter estimation. This tests the faithfulness of the templates. It should be pointed out at the outset that there is a large covariance between the chirp mass and the spin magnitude and a small error in the estimation of the chirp mass is compensated by a large error in the estimation of the spin magnitude. In Fig. 7 we have plotted the percentage bias in the estimation of the chirp-mass for both T- (left panel) and P-approximant (right panel) templates. From Fig. 7, left panel, it is clear that for T-approximants the bias in \mathcal{M} varies between 0 – 5%. Comparing the left and right panels of Fig. 7 we find that the P-approximant templates (right panels) are more faithful with the percentage bias being less than 1% in general.

In Fig. 8 we present the percentage bias in the estimation of the spin magnitude of the central BH. We find that for both approximants we have to endure a large bias in q . Once again the P-approximant templates are more faithful. For T-approximants the bias varies between 5 and 90%, while for P-approximants it lies between 2 and 10%. From the middle and bottom Sections of Fig. 9, it is clear that even in the equal mass case the bias in the estimation of both parameters is greater for T-approximant templates than P-approximants.

It is therefore clear that in the case of prograde orbits, P-approximant templates must be used in any detection strategy. Not only do they achieve higher fitting factors at all spin and mass ranges compared to the T-approximant templates, but they are also more faithful. Let us finally note that the bias in the estimation of spin is larger at low spin values, which is exactly what we found by best fitting the approximate fluxes with the exact fluxes by using q as a free parameter.

D. Retrograde Orbits – Effectualness

In the case of retrograde motion we carried out the same range of tests as in the prograde case. We found that in the case of maximization over t_0 and Φ_0 the overlaps are not as bad. It seems that all templates perform reasonably well for all spin values. This is probably due to the fact that the PN coefficients at higher orders are smaller when $q < 0$ than when $q > 0$. Additionally, retrograde orbits are less bound and, therefore, less relativistic, and again higher order PN corrections do not play as significant a role for retrograde orbits as they do for prograde orbits. At a spin value of $q = -0.25$, the T-approximant templates achieved fitting factors in the range $0.67 \leq FF \leq 0.81$. This falls off to a mean value of ~ 0.54 at $q = -0.95$. The P-approximant templates also perform better in the retrograde case achieving fitting factors in the range $0.47 \leq FF \leq 0.80$ at $q = -0.25$, and between $0.54 \leq FF \leq 0.84$ at $q = -0.95$.

In addition to extrinsic parameters when we maximize over all the intrinsic parameters the fitting factors improve. In fact, in the case of retrograde orbits both templates achieve fitting factors of $FF \geq 0.99$ regardless of the spin magnitude and the chirp mass. There is no surprise here: The retrograde waveforms are still well within the adiabatic regime and are, therefore, modelled well by both templates. From a purely detection point of view, unlike the prograde case, there is no obvious benefit from employing P-approximant templates. For the equal mass system too there is not much difference in the fitting factors of the two families of templates with the exact signal. However, the fitting factor for T-approximants is well below than the corresponding P-approximant template for spin magnitudes $q > 0.5$.

E. Retrograde Orbits – Faithfulness

The benefit of using P-approximant templates for retrograde motion is only observed when we consider parameter extraction. Referring to the bottom portions of the two panels in Fig. 7, we note that the T-approximants perform well at all spins for $3.0 \geq \mathcal{M} \leq 4.5$, with a bias of less than 1% in the estimation of \mathcal{M} . Beyond this, there is in general a bias of $> 2\%$. As we approach the extreme retrograde case the bias rises to as much as 55%. The P-approximants perform in a similar manner. The bias in the region $3 \geq \mathcal{M} \leq 4.5$ is again in general less than 1%. The error does again increase as we head towards the extreme test-mass range, but in this case it reaches a maximum value of 8% as opposed to the 55% seen in the case of the T-approximants.

The pattern observed in the retrograde case is similar to the prograde case with the errors in the T-approximants greater than those in the P-approximants. The error in estimating q reaches a maximum of 80% for T-approximants and 25% for P-approximants. There is a slight difference, however, between the two cases: We observe that there is an asymmetry in the distribution of contour lines. The T-approximant templates suffer a higher error over a larger span of spins in the retrograde case than in the prograde case. This is consistent with the results presented in Ref. [31, 32] where it was shown that the PN approximation waveforms perform worse in the retrograde case. We should, therefore, not be surprised that the errors are greater for retrograde motion. Now, referring once more to the equal mass case, the P-approximant templates outperform their T-approximant counterparts. Even with this, we must again conclude that while on the surface there is no clear case for using P-approximant templates in searching for retrograde motion systems, they should be used because of the lower bias incurred in the estimation of parameters.

F. Schwarzschild Orbits.

While we have presented the maximized fitting factors and percentage errors in the estimation of the chirp-mass for the Schwarzschild case, we have not made any remarks regarding the maximized spin value. In Table II we present a comparison of the maximized spin for both T and P-approximant templates for a selection of systems. We can see from the table that the best overlap is never achieved using the Schwarzschild value for the spin. For T-approximants the best fitting factors are all obtained by using retrograde values for the spin. For P-approximants, it varies between prograde and retrograde values. In general, regardless of whether the maximized spin is a prograde or retrograde value, we can see that the absolute error in the spin value is always smaller for P-approximant templates.

V. CONCLUSIONS

We have applied P-approximant templates to the case of a NS orbiting Kerr BHs of varying mass and spin. When graphically matching the numerical fluxes we found that the P-approximant fluxes gave a better fit as compared to the PN fluxes, especially when we varied the value of the spin parameter and best fitted the exact flux. However, the true test of how well a template performs is reflected by the fitting factors achieved. Using a signal waveform constructed from the exact expression for the orbital energy and numerical fluxes from black hole perturbation theory, we were

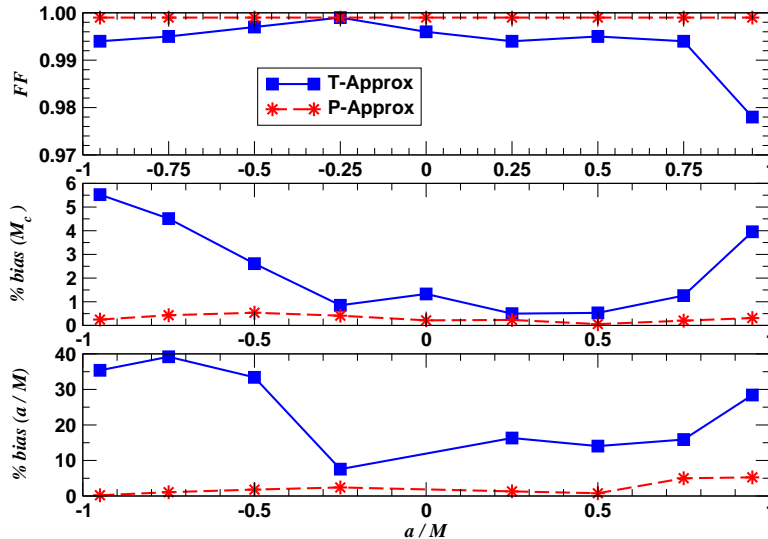


FIG. 9: The fitting factors for a 10-10 M_{\odot} binary - without the finite mass correction terms - for T and P-approximant templates (top). The percentage error in the estimation of the chirp-mass for T and P-approximant templates (middle). The percentage error in the estimation of the spin of the central black hole for T and P-approximant templates (bottom).

TABLE II: Fitting factors for a variety of Schwarzschild systems of various masses. The maximized values of m_1 , m_2 and q are presented in brackets underneath.

(m_1, m_2)	$\langle h_{T_8} h^X \rangle$	$\langle h_{P_8} h^X \rangle$	(m_1^T, m_2^T, q^T)	(m_1^P, m_2^P, q^P)
(1.4, 50)	0.998	0.999	(1.5, 49.0, -0.02)	(1.4, 52.7, +0.06)
(1.4, 45)	0.998	0.999	(1.4, 48.6, -0.08)	(1.4, 46.1, +0.02)
(1.4, 40)	0.997	0.999	(1.5, 37.3, -0.09)	(1.4, 41.5, +0.04)
(1.4, 35)	0.995	0.998	(1.5, 32.8, -0.08)	(1.4, 36.0, +0.03)
(1.4, 30)	0.978	0.996	(1.6, 25.9, -0.15)	(1.4, 30.8, +0.03)
(1.4, 25)	0.991	0.996	(1.5, 22.6, -0.14)	(1.5, 24.9, -0.10)
(1.4, 20)	0.990	0.995	(1.5, 17.9, -0.16)	(1.4, 20.1, -0.01)
(1.4, 15)	0.996	0.997	(1.5, 13.5, -0.14)	(1.4, 15.0, -0.02)
(1.4, 10)	0.996	0.999	(1.6, 8.30, -0.19)	(1.4, 10.0, -0.02)

able to compare the performance of T and P-approximant templates. In the case of retrograde, Schwarzschild and prograde orbits, not only did the P-approximants gave better and more reliable fitting factors, they also gave smaller biases in the estimation of parameters. We also saw the true power of the P-approximant templates in that we were able to generate templates right up to the LSO. This is something that was not possible with the T-approximant templates due to the approximation for the flux function becoming negative before the LSO is reached. This restricted just how much of the numerical waveform we could model. While not being completely correct due to the fact that we omitted the finite-mass correction terms, we also saw that the P-approximant templates gave the best performance when in the equal-mass case.

The bias in the estimation of parameters is particularly poor in the case of T-approximants especially for high-mass systems. Since high-mass systems can be seen to a greater distance, and therefore likely to be the first sources to be detected, it is important to keep in mind that the bias in the estimation of parameters could be as large as the random errors associated with the measurement. Such biases could seriously affect the test of general relativity [58] that are envisaged to be carried out with the aid of high-mass systems. It is clear that for the type of systems examined in this paper, namely equatorial test-mass circular orbits in Kerr, P-approximant templates are to be preferred over their PN counterparts in both detection and measurement. It remains to be seen if P-approximants (or their improved versions) prove to be good enough when considering generic orbits in Kerr and for comparable mass systems with spinning black holes on generic orbits.

Acknowledgments

We would like to thank Prof. M. Shibata for his permission to use the numerical fluxes in this work. We would also like to thank T. Damour, B. Iyer and the members of the Cardiff relativity group for the stimulating conversations and helpful suggestions. EKP would like to thank the School of Physics and Astronomy, Cardiff, for its hospitality in the final stages of this work. This research was supported in parts by the Particle Physics and Astronomy Research Council and the Leverhulme Trust, both in the UK.

-
- [1] A. Abromovici et al., *Science* **256**, 325 (1992)
 - [2] C. Bradaschia et al, *Nucl. Instrum. Methods Phys. Res. Sec. A*, 518 (1990)
 - [3] J. Hough and K. Danzman, *Proposal for a 600m Laser Interferometric Gravitational Wave Antenna*, (1994)
 - [4] K. Kuroda et al in *Gravitational Waves : Sources and Detectors*, ed. by I. Cinfolini and F. Fiducaro, 100 (World Scientific, 1997)
 - [5] L. P. Grishchuk, V. M. Lipunov, K. A. Postnov, M. E. Prokhorov and B. S. Sathyaprakash, *Phys. Usp.* **44**, 1 (2001)
 - [6] E. Phinney, *Astrophys. J.* **380**, L17 (1991)
 - [7] R. Narayan, T. Piran and A. Shemi, *Astrophys. J.* **379**, L17 (1991)
 - [8] I. H. Stairs et al., *Astrophys. J.* **505**, 352 (1998)
 - [9] K. Belczynski, V. Kalogera and T. Bulik, *Astrophys. J.*, **572** 407 (2001). astro-ph/0111452.
 - [10] K. A. Postnov and M. E. Prokhorov, *Binary Black Hole Formation and Mergings*, in proceedings of the XXXIV Rencontres de Moriond "Gravitational waves and experimental Gravity", January 23-30, 1999, astro-ph/9903193.
 - [11] C. W. Helstrom, *Statistical Theory of Signal Detection* (Pergamon Press, London 1968)
 - [12] S. V. Dhurandhar and B. S. Sathyaprakash, *Phys. Rev. D* **49**, 1707 (1994)
 - [13] A. Buonanno, Y. Chen, and M. Vallisneri, *Phys. Rev. D* **67**, 024016 (2003).
 - [14] A. Buonanno, Y. Chen, and M. Vallisneri, *Phys. Rev. D* **67**, 104025 (2003).
 - [15] Y. Pan, A. Buonanno, Y. Chen, and M. Vallisneri, *A physical template family for gravitational waves from precessing binaries of spinning compact objects: Application to single-spin binaries*, gr-qc/0310034
 - [16] L. Blanchet, T. Damour, B. Iyer, C. M. Will and A. G. Wiseman, *Phys. Rev. Lett.* **74**, 3515 (1995)
 - [17] L. Blanchet, T. Damour and B. Iyer, *Phys. Rev. D* **51**, 5360 (1995)
 - [18] C. M. Will and A. G. Wiseman, *Phys. Rev. D* **54**, 4813 (1996)
 - [19] L. Blanchet, B. Iyer, C. M. Will and A. G. Wiseman, *Class. Quantum Grav.* **13**, 575 (1996)
 - [20] L. Blanchet, *Phys. Rev. D* **54**, 1417 (1996)
 - [21] T. Damour, P. Jaranowski and G. Schäfer, *Phys. Rev. D* **63**, 044021 (2001); V. C. de Andrade, L. Blanchet and G. Faye, *Class. Quantum Grav.* **18**, 753, (2001).
 - [22] L. Blanchet, G. Faye, B. R. Iyer and B. Joquet, *Phys. Rev. D* **65**, 061501 (2002); L. Blanchet, B. R. Iyer and B. Joquet, *Phys. Rev. D* **65**, 064005 (2002)
 - [23] E. Poisson, *Phys. Rev. D* **47**, 1497 (1993)
 - [24] C. Cutler, L. S. Finn, E. Poisson and G. J. Sussman, *Phys. Rev. D* **47**, 1511 (1993)
 - [25] H. Tagoshi and T. Nakamura, *Phys. Rev. D* **49**, 4016 (1994)
 - [26] M. Sasaki, *Prog. Theor. Phys.* **92**, 17 (1994)
 - [27] H. Tagoshi and M. Sasaki, *Prog. Theor. Phys.* **92**, 745 (1994)
 - [28] T. Tanaka, H. Tagoshi and M. Sasaki, *Prog. Theor. Phys.* 1087 (1996)
 - [29] P. R. Brady, J. D. E. Creighton and K. S. Thorne, *Phys. Rev. D* **58**, (1998)
 - [30] E. Poisson, *Phys. Rev. D* **49**, 1860 (1993)
 - [31] M. Shibata, M. Sasaki, H. Tagoshi and T. Tanaka, *Phys. Rev. D* **51**, 1646 (1995)
 - [32] H. Tagoshi, M. Shibata, T. Tanaka and M. Sasaki, *Phys. Rev. D* **54**, 1439 (1996)
 - [33] C. Cutler et al., *Phys. Rev. Lett.* **70**, 2984 (1993)
 - [34] E. Poisson, *Phys. Rev. D* **52**, 5719 (1995)
 - [35] E. Poisson, *Phys. Rev. D* **55**, 7980 (1997)
 - [36] T. Damour, B. R. Iyer and B. S. Sathyaprakash, *Phys. Rev. D* **57**, 885 (1998)
 - [37] E. K. Porter, *Class. Quantum Grav.* **19**, 4343, (2002)
 - [38] Y. Mino, M. Sasaki, M. Shibata, H. Tagoshi and T. Tanaka *Prog. Theor. Phys. Suppl.* **128** 1 (1997).
 - [39] A. Buonanno and T. Damour, *Phys. Rev. D* **59**, 084006 (1999)
 - [40] T. Damour, *Phys. Rev. D* **64**, 124013 (2001)
 - [41] T. Damour, B. R. Iyer and B. S. Sathyaprakash, *Phys. Rev. D* **63**, 044023 (2001)
 - [42] T. Damour, B. R. Iyer, P. Jaranowski and B. S. Sathyaprakash, *Phys. Rev. D* **67**, 064028 (2003)
 - [43] K. S. Thorne, *Gravitational Radiation*, in S. W. Hawking and W. Israel (eds), *300 Years of Gravitation* (Cambridge Uni. Press, Cambridge)
 - [44] B. S. Sathyaprakash and S. V. Dhurandhar, *Phys. Rev. D* **44**, 3819 (1991)
 - [45] S. V. Dhurandhar, J. Watkins and B. F. Schutz, *Fourier transform of a coalescing binary signal* (Unpublished preprint,

- 1989)
- [46] T. Damour, B. R. Iyer and B. S. Sathyaprakash, *Phys. Rev. D* **62**, 084036 (2000)
 - [47] B. S. Sathyaprakash, *Phys. Rev. D* **50**, R7111 (1994)
 - [48] W. H. Press, B. P. Flannery, S. A. Teukolsky and W. T. Vetterling, *Numerical Recipes in C : The Art of Scientific Computing* (Cambridge Uni. Press, Cambridge 1992) 2nd Edition.
 - [49] C. M. Bender and S. A. Orszag, *Advanced Mathematical Methods for Scientists and Engineers*, McGraw-Hill International Book Company, Singapore, 1978.
 - [50] J. M. Bardeen, W. H. Press and S. A. Teukolsky, *Astrophys. J.* **178**, 374 (1972)
 - [51] S. Chandrasekhar, *The Mathematical Theory of Black Holes* (Oxford Uni. Press, New York, 1983)
 - [52] M. Shibata (private communication)
 - [53] C. Cutler and E. Flanagan, *Phys. Rev. D* **49** 2658 (1994) gr-qc/9402014.
 - [54] R. Balasubramanian, B. S. Sathyaprakash, and S. V. Dhurandhar, *Phys. Rev. D* **53**, 3033 (1996);
 - [55] B. J. Owen, *Phys. Rev. D* **53**, 6749 (1996);
 - [56] B. J. Owen and B. S. Sathyaprakash, *Phys. Rev. D* **60**, 022002 (1999).
 - [57] B. F. Schutz in *The Detection of Gravitational Radiation*, ed. by D. Blair (Cambridge Uni. Press, Cambridge 1989)
 - [58] L. Blanchet and B. S. Sathyaprakash, *Phys. Rev. Lett.* **74**, 1067 (1995).
 - [59] We shall work in a system of units in which the speed of light and Newton’s gravitational constant are both set equal to unity: $c = G = 1$.
 - [60] Note that the expected PSD for GEO600 has changed over the years. However, we continue to use the “design” sensitivity curve in order to make it easier for comparing the results of this study with previous studies.
 - [61] The expression for the SNR in this paper differs from that in Ref. [46] by a factor $\sqrt{2}$ because here we use one-sided PSD as opposed to two-sided PSD used in Ref. [46].
 - [62] The divergence referred to here is the behaviour of the successive orders of the Taylor expansion of the flux which might not converge as we go to higher orders.
 - [63] Note that the post-Newtonian coefficients of flux in are taken from Ref. [32] Eq. (G19). We have confirmed with Tagoshi et al. that the term $359\pi q/14$ has the wrong sign in some later references but Ref. [32] has the correct sign.
 - [64] Indeed, it has been known [36, 42] that occasionally spurious poles occur very close to the zeroes of the function so much so that the two could cancel each other but for a very slight difference in their locations. In such cases one cure would be to remove both the pole and the zero by hand if they occur sufficiently close to each other.
 - [65] While using approximate templates to detect a truly general relativistic signals a bias in the estimation of parameters is inevitable. This is because, as noted while studying the effectualness of templates, the template shape is not identical to that of the signal when the intrinsic parameters are matched. Consequently, higher overlaps can be achieved by mismatching the template parameters relative to the signal. Since matched filtering isolates the template that obtains the best signal-to-noise ratio, there will be a bias in the estimation of parameter.

APPENDIX A: PADÉ APPROXIMATION

Let $f(x)$ be an analytic function whose Taylor expansion in x , denoted $T_n(x)$, is $T_n(x) = \sum_{k=0}^n a_k x^k$.

We construct the Padé Approximation $P_M^N(x)$ of $T_n(x)$ by equating the polynomial expansion with a rational function to the same order according to

$$T_n(x) = P_M^N(x) \equiv \frac{B_N(x)}{D_M(x)}, \quad (\text{A1})$$

where

$$\frac{B_N(x)}{D_M(x)} = \frac{\sum_{n=0}^N b_n x^n}{\sum_{n=0}^M d_n x^n}, \quad (\text{A2})$$

such that $n+1 = N+M+1$. The benefit of using Padé Approximants over Taylor Approximants is that the error in the approximation after L terms reduces by a factor of 2^L [49]. If we let $M = N + \epsilon$, where $\epsilon = 0$ or 1 , we construct the “diagonal” and “sub-diagonal” Padé Approximants respectively. The advantage of this is that we can cast the rational function in the form of a continued fraction, i.e.

$$P_{N+\epsilon}^N = \frac{c_0}{1 + \frac{c_1 x}{1 + \frac{c_2 x}{\ddots}}}. \quad (\text{A3})$$

If we use the rational function interpretation, Eq. A2, each time we go to a higher order n of approximation, we have to recalculate each of the coefficients, b_n and d_n . However, by using the continued fraction formalism, we only have to calculate the newest coefficient, c_n . As an example, consider the Taylor expansion

$$T_n(v) = a_0 + a_1(v). \quad (\text{A4})$$

By matching this to a Padé Approximation of the same order we get

$$a_0 + a_1 v = \frac{c_0}{1 + c_1 v}. \quad (\text{A5})$$

Solving for the Padé coefficients, c_n , gives us

$$c_0 = a_0 \quad , \quad c_1 = -\frac{a_1}{a_0}. \quad (\text{A6})$$

If we now go to the next order, i.e.

$$a_0 + a_1 v + a_2 v^2 = \frac{c_0}{1 + \frac{c_1 v}{1 + c_2 v}}, \quad (\text{A7})$$

and solve for the coefficients c_n once more, we obtain

$$c_0 = a_0 \quad , \quad c_1 = -\frac{a_1}{a_0} \quad , \quad c_2 = -\frac{a_2}{a_1} + \frac{a_1}{a_0}. \quad (\text{A8})$$

The example shows that as we go to higher and higher orders in v , we only have to calculate one new coefficient as all the lower order coefficients remain constant. Consequently, there is a sense of stability in the behaviour of the continued fraction coefficients and convergence is easier to test.

There are, unfortunately, problems with Padé approximation that one should bear in mind: Firstly, there are regions where Padé approximants diverge while Taylor Approximants converge. The second, and perhaps most important feature is that when Padé approximation does indeed converge, we cannot be sure that it converges to the exact function that we had in mind [48]. It should therefore always be kept in mind that there are inherent difficulties in using Padé Approximants. Finally, Padé approximants sometimes exhibit spurious poles in the region of interest. However, as one will be able to test *a priori* the existence of poles one can avoid the use of such approximants.